Identification of circular RNA biomarkers for Pien Tze Huang treatment of CCl_4-induced liver fibrosis using RNA-sequencing

TING WANG[1*], JINHANG ZHU[1*], LONGHUI GAO[1,2], MUYUN WEI[1], DI ZHANG[1], LUAN CHEN[1], HAO WU[1], JINGSONG MA[1], LIXING LI[3], NA ZHANG[1], YANJING WANG[4], QINGHE XING[5], LIN HE[1,6], FEI HONG[2] and SHENGYING QIN[1,7]

[1]Bio-X Institutes, Key Laboratory for The Genetics of Developmental and Neuropsychiatric Disorders (Ministry of Education), Shanghai Jiao Tong University, Shanghai 200030; [2]Fujian Provincial Key Laboratory of Pien Tze Huang Natural Medicine Research and Development, Zhangzhou Pien Tze Huang Pharmaceutical Co., Ltd., Zhangzhou, Fujian 363000; [3]Department of General Surgery, Shanghai General Hospital, School of Medicine, Shanghai Jiao Tong University; [4]State Key Laboratory of Microbial Metabolism, Joint Laboratory of International Cooperation in Metabolic and Developmental Sciences, School of Sciences and Biotechnology, Shanghai Jiao Tong University, Shanghai 200240; [5]Institutes of Biomedical Sciences and Children's Hospital, Fudan University, Shanghai 201102; [6]Baoan Maternal and Child Health Hospital, Jinan University, Shenzhen, Guangdong 518101; [7]Collaborative Innovation Center, Jining Medical University, Jining, Shandong 272013, P.R. China

Received March 26, 2021; Accepted October 26, 2021

DOI: 10.3892/mmr.2022.12825

Abstract. Pien Tze Huang (PZH), a common hepatoprotective Traditional Chinese Medicine that has been found to be an effective treatment for carbon tetrachloride-induced hepatic damage, including liver fibrosis. Circular RNAs (circRNAs) serve a crucial role in regulating gene expression levels via circRNA/micro (mi)RNA/mRNA networks in several human diseases and biological processes. However, whether circRNAs are involved in the underlying mechanism of the therapeutic effects of PZH on liver fibrosis remains unclear. Therefore, the aim of the present study was to investigate these effects using circRNA expression profiles from PZH-treated fibrotic livers in model mice. A case-control study on >59,476 circRNAs from CCl_4-induced (control group, n=6) and PZH-treated (case group, n=6) mice was performed using circRNA sequencing in liver tissues. PZH treatment resulted in the differential expression of 91 circRNAs, including 58 upregulated and 33 downregulated circRNAs. Furthermore, the construction of competing endogenous networks also indicated that differentially expressed circRNAs acted as miRNA sponges. Gene Ontology and Kyoto Encyclopedia of Genes and Genomes pathway enrichment analysis of miRNA targets demonstrated that PZH-affected circRNAs were mainly involved in biological processes such as 'positive regulation of fibroblast proliferation', 'cellular response to interleukin-1' and 'regulation of DNA-templated transcription in response to stress' and in a number of important pathways, such as 'TNF signaling pathway', 'PI3K-Akt signaling pathway', 'IL-17 signaling pathway' and 'MAPK signaling pathway'. To further validate the bioinformatics data, reverse transcription-quantitative PCR was performed on seven miRNA targets in a human hepatic stellate LX-2 cell model. The results suggested that seven of the miRNAs exhibited regulatory patterns that were consistent with those of the transcriptome sequencing results. Kaplan-Meier survival analysis demonstrated that the expression levels of dihydrodiol dehydrogenase and solute carrier family 7, member 11 gene were significantly associated with patient survival, 269 patients with liver hepatocellular carcinoma from The Cancer Genome Atlas database. To the best of our knowledge, this was the first study to provide evidence that PZH affects circRNA expression levels, which may serve important roles in PZH-treated fibrotic liver through the regulation of functional gene expression. In conclusion, the

Correspondence to: Professor Fei Hong, Fujian Provincial Key Laboratory of Pien Tze Huang Natural Medicine Research and Development, Zhangzhou Pien Tze Huang Pharmaceutical Co., Ltd., 50-1 Xinhua North Road, Xiangcheng, Zhangzhou, Fujian 363000, P.R. China
E-mail: pzhhf123@126.com

Professor Shengying Qin, Bio-X Institutes, Key Laboratory for The Genetics of Developmental and Neuropsychiatric Disorders (Ministry of Education), Shanghai Jiao Tong University, 1954 Hua Shan Road, Shanghai 200030, P.R. China
E-mail: chinsir@sjtu.edu.cn

*Contributed equally

Abbreviations: CCl_4, carbon tetrachloride; ceRNA, competing endogenous RNA; circRNA, circular RNA; ECM, extracellular matrix; GO, Gene Ontology; KEGG, Kyoto Encyclopedia of Genes and Genomes; miRNA/miR, microRNA; PZH, Pien Tze Huang; RT-qPCR, reverse transcription-quantitative PCR; seq, sequencing

Key words: liver fibrosis, Pien Tze Huang, circular RNAs, RNA-sequencing, bioinformatics analysis

present study provided new insights into the mechanism underlying the pathogenesis of liver fibrosis and identified potential novel, efficient, therapeutic targets against liver injury.

Introduction

Liver fibrosis may be caused by acute or chronic liver injury and has been associated with severe morbidity and mortality (1). The progression from hepatitis to liver fibrosis, cirrhosis and even hepatic carcinoma has been reported to be accelerated by the occurrence of metabolic liver disease, alcoholism and viral hepatitis (2,3). The development of liver fibrosis is a result of the interaction among various types of resident hepatocytes, inflammatory cells, mediators and extracellular matrix (ECM) components, which are usually characterized by increased matrix protein production and decreased matrix remodeling (4,5). Liver fibrosis accelerates the progression of acute liver disease to its chronic form by disrupting the normal liver parenchyma (6). Furthermore, animal models that simulate liver fibrosis have improved our understanding of liver injury, and carbon tetrachloride (CCl_4)-induced liver fibrosis is widely used in mouse models to study hepatotoxic mechanisms (3,7). CCl_4-induced acute liver injury leads to the complex regulation of cellular responses. It has previously been established that continuous exposure of mice to a low dose of CCl_4 (0.2 ml/kg), beginning at 8 weeks of age and lasting up to 6 weeks, leads to the development of liver fibrosis and compensatory cell proliferation (8). A CCl_4-induced liver fibrosis mouse model has been demonstrated to be able to effectively simulate the formation of liver injury *in vivo*, which has been widely used in the study of the mechanism of hepatotoxicity (3,8-11).

Currently, treatments for liver fibrosis mainly include eliminating the primary causes and suppressing inflammation. However, there is still a lack of effective preventative methods or therapeutic drugs for liver fibrosis (12,13). The drug discovery process has paid great attention to the investigation of the efficacy drugs used in traditional medicine, as they are cheaper and have fewer side effects. Pien Tze Huang (PZH), a complex combination of *Panax notoginseng* (85%); *Calculus bovis* (5%); snake gallbladder (7%), obtained from the dry gall bladder of snake; and musk (3%), obtained from the preputial gland located in the abdomen of male musk deer, has been used as a traditional medicine with anti-inflammatory and soothing effects on skin boils and abscesses (14). A previous study has demonstrated that PZH exerts an important protective effect on CCl_4-induced liver injury in mice (15). Additional studies have also suggested that PZH is effective in inhibiting liver damage caused by excessive drinking (16), improving histopathological damage in the liver and positively affecting physiological and biochemical indexes, such as serum alanine aminotransferase and aspartate aminotransferase, to a certain extent (15,17). Cell necrosis and swelling, microvesicular steatosis and lymphocyte infiltration in the injured liver have been reported to be significantly reduced following PZH treatment for liver disease (18).

Circular RNAs (circRNAs) are a recently discovered type of non-coding RNAs (ncRNAs). Most circRNAs are endogenous ncRNAs, and their formation does not have a covalent ring structure at the 3' and 5' end (19). Owing to their special structure, circRNAs cannot be easily degraded by nucleic acid exoenzyme ribonuclease R (RNase R) and are more stable than linear RNA (20). Furthermore, circRNAs regulate alternative splicing and transcription in a variety of diseases by acting as efficient microRNA (miRNA/miR) sponges, which can efficiently prevent the suppression of their mRNA targets (21,22). A previous study confirmed the regulatory role of circRNAs in circRNA/miRNA-gene regulatory networks by building a database of circRNAs derived from transcriptome sequencing data (23). Therefore, the interactions among circRNA, miRNA and mRNA have been considered important in transcriptional and post-transcriptional regulation.

An increasing number of studies have demonstrated that circRNAs can act as promising and technically suitable biomarkers for the occurrence and development of various diseases (24-28). Recently, Xu *et al* (29) analyzed the regulatory role of the circRNA/miRNA/mRNA network and revealed that circRNA_0001178 and circRNA_0000826 may be potential diagnostic markers for colorectal cancer metastasis. Furthermore, a recent study revealed that *Mus musculus* (mmu)_circRNA_002381 may influence the regulatory process of the transcription of certain genes affected by cocaine-induced neuroplasticity via the circRNA/miRNA interaction network (30). However, it remains unclear as to how the circRNA/miRNA/mRNA network modulates improvements in the fibrotic liver tissue of PZH-treated subjects.

The present study investigated the hepatoprotective activity of PZH against CCl_4-induced liver fibrosis, and aimed to determine the circRNA-based molecular mechanisms by which it may confer its protection on the mice liver against CCl_4-induced liver damage. Differentially expressed circRNAs were successfully identified using high-throughput RNA-sequencing (RNA-seq) in liver tissues from CCl_4-induced and PZH-treated mice. The sponging action of differentially expressed circRNAs and related miRNA targets was further examined using multiple bioinformatics tools. Moreover, functional circRNA/miRNA/mRNA networks were established to provide novel insights into the treatment of liver fibrosis with PZH. The functional characteristics of the representative circRNA candidates were further analyzed by performing reverse transcription-quantitative PCR (RT-qPCR) on the mRNAs associated with the differentially expressed circRNAs in hepatic stellate cells (HSCs).

Materials and methods

Animal experiment. A total of 45 C57BL/6 mice of each group (age, 6 weeks; weight, 20-30 g) were purchased from Shanghai Model Organisms Center, Inc. The mice were housed at 24±2˚C, relative humidity of 55±15%, kept in clean cages under a 14/10 h light-dark cycle and fed with standard rodent diet throughout the entire experimental period. Mice were randomly divided into two groups named the 'PZH-treated' and 'CCl_4-induced' (PZH-treated, hepatic fibrosis model using PZH plus CCl_4; CCl_4-induced, hepatic fibrosis model using CCl_4 only; n=15 mice/group). Meanwhile, a no-induction group (n=15 mice/group) was added to confirm the success of the liver fibrosis model. Mice in the CCl_4-induced liver fibrosis model group were intraperitoneally injected with a solvent mixture of 10 μl/g body weight CCl_4 (Wuhan Yafa Biological Technology Co., Ltd.) and 10% corn oil twice a week and

intragastrically administered with double-distilled (dd)H_2O once a day. Mice in the PZH-treatment group were intraperitoneally injected with a solvent mixture of 10 μl/g body weight CCl_4 and 10% corn oil twice a week (31) and intragastrically administered with 0.25 mg/g PZH-sonicated reagent (Zhangzhou Pientzehuang Pharmaceutical Co., Ltd.; Chinese Food and Drug Administration approval no. Z35020242; the PZH drug powder was dissolved in double distilled water, and its concentration was diluted to 25 mg/ml) once a day. During the 8-week experimental period, three mice in each group were anesthetized intraperitoneally with 40 mg/kg pentobarbital (Sigma-Aldrich; Merck KGaA) and sacrificed by cervical dislocation every 2 weeks in the first 6 weeks, and their liver tissue and blood were harvested for detecting the hepatic fibrosis level and hepatic biochemical index. The remaining 12 mice were also anesthetized and sacrificed by cervical dislocation in the 8th week. Mice were subsequently subjected to a laparotomy and liver tissue was harvested for the following experiments. Throughout the animal experiment mental state, hair and the body weight of the mice were closely monitored for toxic effects caused by CCl_4. No significant differences were observed in the body weight of the mice between CCl_4-induced and PZH-treated groups (P=0.7772; Fig. S1). The experimental procedures in the present study were approved by The Institutional Review Board of Shanghai Jiao Tong University (Shanghai, China; approval no. IACUC. NO:2017-0033).

RNA isolation for high-throughput sequencing. Total RNA was extracted from mouse liver tissue samples using TRIzol® reagent (Thermo Fisher Scientific, Inc.) according to the manufacturer's protocol. Samples were then processed with RNase-free DNase to remove traces of genomic DNA. The RNA concentration and quality were determined using a NanoDrop® ND-2000 spectrophotometer (Thermo Fisher Scientific, Inc.) and the Bioanalyzer 2100 System (Agilent Technologies, Inc.). The A260/A280 ratio and RNA integrity number (RIN; Agilent Technologies Deutschland GmbH) were used to assess RNA purity and integrity, respectively (32). All samples met the following criteria: A260/A280 ratio >1.8 and RIN >8, which means that the RNA integrity was high quality for sequencing.

Transcriptome data analysis. RNA libraries were constructed using ribosomal RNA-depleted RNAs with TruSeq Stranded Total RNA Library Prep Kit (cat. no. RS-122-2201; Illumina, Inc.) according to the manufacturer's protocol. Briefly, 5 μg RNA was treated using the Ribo-Zero™ kit (cat. no. MRZH11124; Illumina, Inc.) to remove all ribosomal RNAs and linear RNAs were digested using RNase R (cat. no. RNR07250; Lucigen Corporation). Subsequently, the enriched circRNAs were fragmented and a double-stranded cDNA library was synthesized using random primers and adapters. Finally, the cDNAs were purified and amplified with a thermocycler. All samples were mixed and underwent bridge amplification to generate clusters using HiSeq 4000 Paired-End Cluster Kit (cat. no. PE-410-1001-1; Illumina, Inc.). Quality control was performed using Q30. The library was subjected to 150-bp paired-end sequencing using HiSeq 4000 SBS Kit (cat. no. FC-410-1001-1; Illumina, Inc.). FastQC (version v0.11.5; http://www.bioinformatics.babraham.ac.uk/projects/fastqc) (33) was used to evaluate the quality of the sequencing data. Trim-galore (version 0.6.0) (34) with default parameters was used to remove double-ended adapters and perform quality control on raw sequencing data.

Identification of differentially expressed circRNAs between the two groups. The filtered data were first mapped to the reference genome/transcriptome (version mm10, downloaded from UCSC, https://genome.ucsc.edu/) using STAR software version 2.5.3 (35). Only the common circRNAs predicted by CIRI (version 2.0.6) (36) and CIRCexplorer (37) software were termed 'identified circRNAs' in the subsequent analysis. CircBase (http://www.circbase.org/) (38) and Circ2Traits (39) (http://gyanxet-beta.com/circdb) databases were used to annotate the identified circRNAs. circRNAs were normalized to the number of back-splice junctions spanning spliced reads per billion mapping (SRPBM). The differentially expressed circRNAs were screened according to a $\log_2$(FC)>1 and P<0.05. RNA-seq data were deposited in National Center for Biotechnology Information Gene Expression Omnibus (GEO; accession no. GSE150883).

Target prediction and bioinformatics analysis. For the specific competing endogenous RNA (ceRNA) network of significantly dysregulated circRNAs and mRNAs, the miRNA/mRNA and miRNA/circRNA interactions were predicted using the RegRNA 2.0 (40) (http://regrna2.mbc.nctu.edu.tw/), miRWalk 2.0 (41) (http://mirwalk.umm.uni-heidelberg.de) and TargetScan 7.2 (42) (http://www.targetscan.org) databases. miRNA-binding sites on circRNAs were determined using RegRNA 2.0 with a cutoff score of ≥170 and free energy of ≤-25. The putative target genes of these miRNAs were identified using the miRWalk algorithm with a binding energy of ≤-30 (43). The intersection of predicted target genes identified by both of these algorithms was selected as the differentially expressed circRNA-related predicted target genes in the present study for further analysis. The shared mRNAs between the differentially expressed circRNA-related predicted target genes in the present study and the differentially expressed mRNAs from mRNA-seq data (GEO accession no. GSE133481) were extracted. The overlapping mRNA-related miRNAs and miRNA binding sites on these circRNAs were selected to construct the ceRNA regulatory network. Cytoscape (version 3.6.1) was used to visualize the circRNA/miRNA/mRNA network interactions (44). The R package Cluster Profiler (45) was used for Gene Ontology (GO) analysis (http://geneontology.org/) and the Kyoto Encyclopedia of Genes and Genomes (KEGG) database (https://www.kegg.jp/) was used for pathway analysis of the differentially expressed circRNA-related target genes based on the adjusted P<0.05.

Validation of differentially expressed circRNA-related target gene candidates by RT-qPCR in LX-2 cells. The expression levels of candidate differentially expressed circRNA-related target genes in the ceRNA network were further validated by RT-qPCR in the human hepatic stellate LX-2 cell line (American Type Culture Collection). LX-2 cells were grown in an incubator with 5% CO_2 at 37˚C in DMEM (Thermo Fisher

Table I. Quality control results for all samples.

Sample	Reads count	Base count	Error, %[a]	Q20, %[b]	Q30, %	GC, %[c]
PZH_1	81068764	10516643897	0.0118	98.28	95.46	57.29
PZH_2	90141456	11798532726	0.0119	98.25	95.41	57.20
PZH_3	85539612	11098006475	0.0118	98.29	95.48	57.46
PZH_4	89396344	11600890156	0.0121	98.17	95.16	57.57
PZH_5	89704690	11682502150	0.0121	98.14	95.14	57.70
PZH_6	82737206	10730442091	0.0119	98.26	95.42	57.13
Control_1	95957422	12581967724	0.0120	98.16	95.26	52.03
Control_2	79748818	10401728633	0.0122	98.06	95.04	55.98
Control_3	88915072	11546488853	0.0120	98.19	95.28	56.98
Control_4	89463266	11634186983	0.0120	98.12	95.26	52.62
Control_5	99444270	12929236537	0.0119	98.18	95.36	54.19
Control_6	82923014	10776422218	0.0122	97.98	94.95	53.67

[a]Percentage of bases with a Phred value >20/total bases; [b]base error rate; [c]the sum of the number of G and C bases as a percentage of the total number of bases. PZH, Pien Tze Huang.

Scientific, Inc.) supplemented with 10% FBS (MilliporeSigma), 2 mM l-glutamine, 100 U/ml penicillin and 100 μg/ml streptomycin (complete medium; Gibco; Thermo Fisher Scientific, Inc.). Cells were seeded into 6-well plates ($1x10^6$/well) and divided into the PZH-induced (0.75 mg/ml) and the untreated control groups. The expression levels of differentially expressed circRNA-related target gene candidates were determined at 24, 48 and 72 h. Total RNA was extracted from LX-2 cells using TRIzol reagent, aforementioned. Total RNA was reversed transcribed into cDNA using 1 μg isolated RNA with the PrimeScript First Strand cDNA Synthesis Kit (Takara Bio, Inc.) according to the manufacturer's protocol. qPCR was subsequently performed using an ABI7500 Real-Time PCR System (Thermo Fisher Scientific, Inc.) and the FastStart Universal SYBR Green Master (Roche Diagnostics). Each qPCR reaction contained 25 μl FastStart Universal SYBR Green Master, 0.3 μM forward primer, 0.3 μM reverse primer, 50 ng cDNA template and ddH_2O to a final volume of 50 μl. The qPCR conditions were as follows: Initial denaturation at 95˚C for 10 min; followed by 40 cycles at 95˚C for 15 and 60 sec at 60˚C. All primers are shown in Table SI. Relative mRNA expression levels were quantified using the $2^{-\Delta\Delta Cq}$ method and normalized to the internal reference gene GAPDH (46). At $2^{-\Delta\Delta Cq}>1$, the mRNA expression levels were considered to be upregulated and at $2^{-\Delta\Delta Cq}<1$ downregulated.

Statistical analysis. Data from three independent experiments were used for analysis. Data are presented as the mean ± SEM. GraphPad Prism 8.0 (GraphPad Software, Inc.) was used for all statistical analyses. Unpaired Student's t-test and one-way ANOVA with Duncan's post hoc test were used to determine the statistical differences between the control and PZH-treated groups. $P<0.05$ was considered to indicate a statistically significant difference.

Survival analysis. Survival analysis was performed using the survival package in R (version 3.6.3) (47) to explore the relationship between the differentially expressed circRNA-related targets and the status data of 269 clinical patients with liver hepatocellular carcinoma from The Cancer Genome Atlas (TCGA) database (48). Patients with expression levels higher than the median values were assigned to the high-expression group, and patients with expression levels lower than the median values were assigned to the low-expression group. Kaplan-Meier survival analysis was performed to plot survival curves and the log-rank test was used to assess the statistical difference in survival rates between the high- and low-expression groups. $P<0.05$ was considered to indicate a statistically significant difference.

Results

Prediction and expression analysis of circRNAs. To identify differentially expressed circRNAs in PZH-treated mice exhibiting liver damage improvement compared with the CCL_4-induced group, RNA-seq was used to profile circRNA expression levels in the tissue samples from six PZH-treated mice and six CCL_4-induced mice with liver fibrosis. The quality control results from the sequencing data demonstrated that the Q30 of all samples reached 95% (Table I). The filtered data was subsequently mapped to the reference genome/transcriptome (GRCm38/mm10; Table II). CIRI and CIRCexplorer software were used to identify the circRNAs in all samples. Detailed information regarding the circRNAs identified is displayed in Table SII. A total of 59,476 intersection circRNAs were detected by circRNA-seq. Among all the types of circRNA, the proportion of exon circRNA was as high as 98.35% (Table SII). Subsequently, hierarchical clustering was performed using an expression matrix calculated from each circRNA across 12 samples. The CCL_4-induced and PZH-treated fibrotic liver samples were classified into different branches (Fig. 1). The SRPBM expression values of each circRNA for all samples are shown in Table SIII.

Table II. Mapping ratio statistics of all clean data.

Sample	Reads count	Mapped reads	Mapped ratio, %	Unique mapped reads	Unique mapped ratio, %
PZH_1	40534382	38952915	96.10	12552203	30.97
PZH_2	45070728	43433153	96.37	14150855	31.40
PZH_3	42769806	41221377	96.38	12478538	29.18
PZH_4	44698172	42680427	95.49	13259939	29.67
PZH_5	44852345	43051071	95.98	12857153	28.67
PZH_6	41368603	39789422	96.18	12193014	29.47
Control_1	47978711	42105288	87.76	14914179	31.08
Control_2	39874409	36838848	92.39	11268513	28.26
Control_3	44457536	42229515	94.99	13088832	29.44
Control_4	44731633	39892267	89.18	13676170	30.57
Control_5	49722135	45379494	91.27	15213018	30.60
Control_6	41461507	37464042	90.36	12430113	29.98

PZH, Pien Tze Huang.

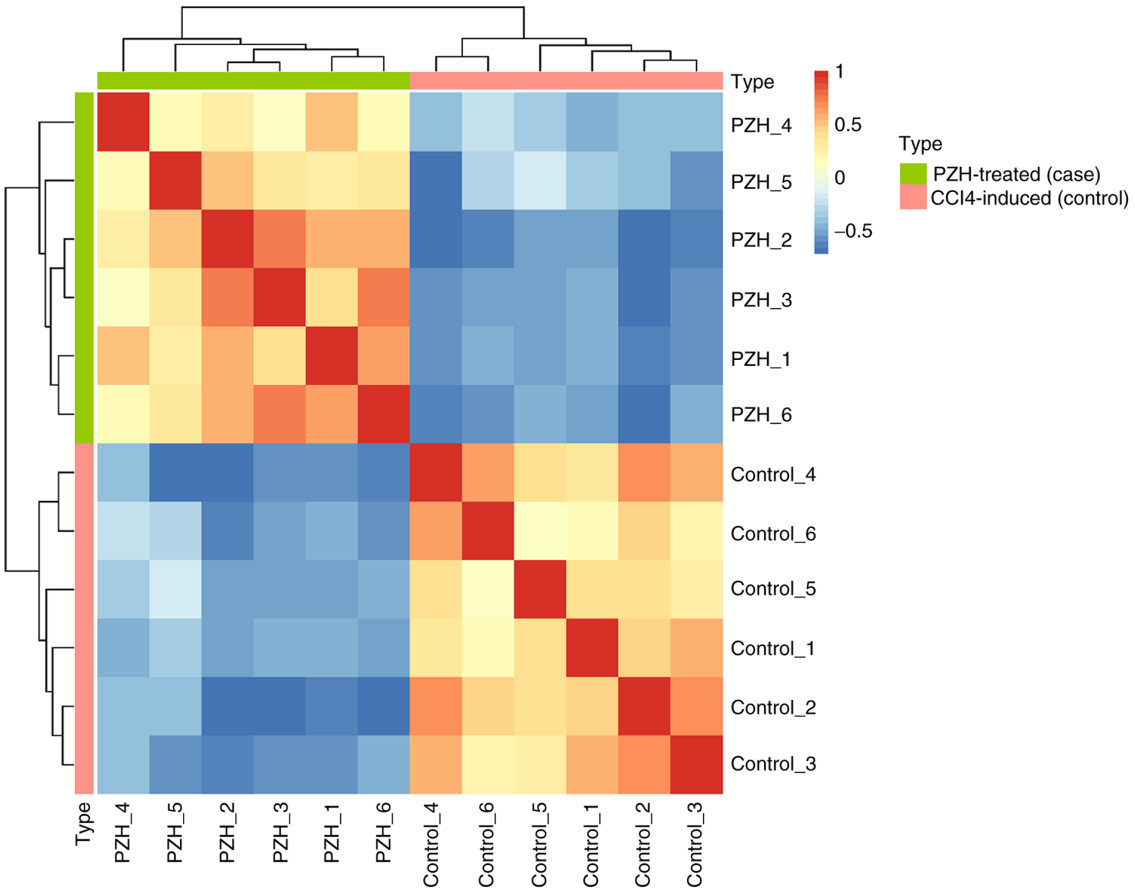

Figure 1. Hierarchical clustering of liver tissues treated with and without PZH. Clustering between samples was performed based on the correlation coefficient values. Each column and row indicates an independent sample. The mean was set to 0, and the standard deviation was set to 1 in the calculation of the $\log_2$ (FPKM+1) value of each gene in the 12 samples. Red represents a positive correlation and blue a negative correlation. PZH, Pien Tze Huang.

Identification of differentially expressed circRNAs. The overall expression profiles of the differentially expressed circRNAs between the CCl_4-induced and PZH-treated groups are displayed in the volcano plot in Fig. 2C. In total, 91 circRNAs, including 58 (63.73%) upregulated and 33 (36.27%) downregulated circRNAs, were demonstrated to be significantly differentially expressed in liver tissue samples from the PZH-treated compared with the CCL_4-induced group (Fig. 2A). An analysis of the source of these circRNAs revealed that, of the 91 differentially expressed circRNAs, 88 (96.7%)

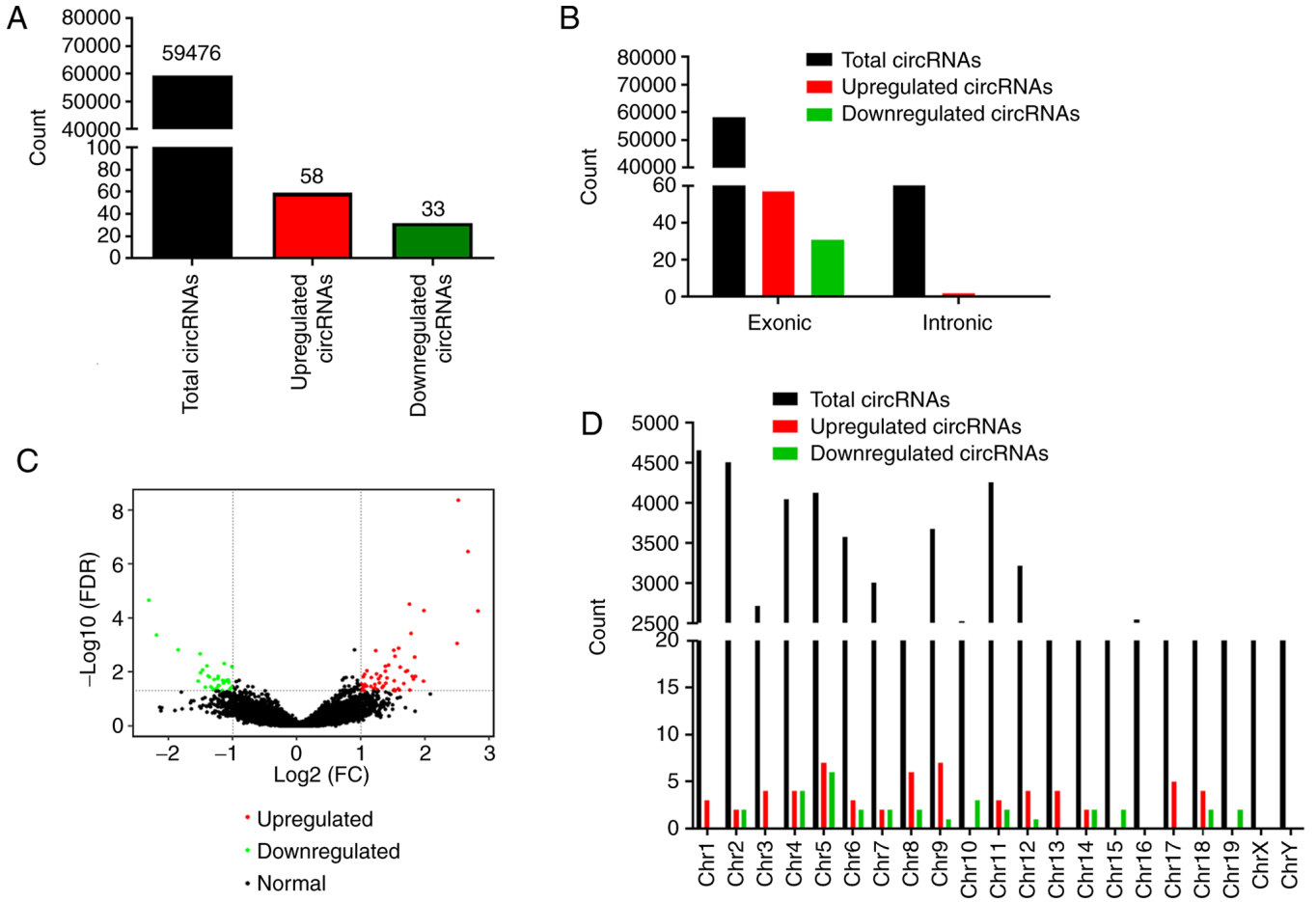

Figure 2. RNA-sequencing analysis of differentially expressed circRNAs in the fibrotic liver of mice treated with or without PZH. (A) Total number of circRNAs and differentially expressed circRNAs in the PZH-treated group. (B) CircRNAs were classified by category. (C) Volcano plots displaying the differentially expressed circRNAs. The horizontal black dotted line corresponds to a -$\log_{10}$(FDR) of 0.05. (D) Distribution of circRNAs in mouse chromosomes. chr, chromosome; circRNAs, circular RNAs; FC, fold-change; FDR, false discovery rate; PZH, Pien Tze Huang.

were derived from exons (data not shown). The results also demonstrated that the most significant differentially expressed circRNAs were transcribed from the exons of protein-coding regions (Fig. 2B). The distribution of the identified circRNAs on different chromosomes was also analyzed. The statistical analysis results demonstrated that circRNAs were distributed on all chromosomes. Moreover, all differentially expressed circRNAs were found to be markedly expressed, except for those on chromosome 16 (Fig. 2D). Hierarchical clustering was also performed to investigate these differentially expressed circRNAs across 12 samples between PZH-treated and CCL_4-induced groups (Fig. 3). Detailed information on the top 20 differentially expressed circRNAs is included in Table SIV. The analysis of the circRNA-seq data suggested that the expression levels of circRNA differed between PZH treatment and CCL_4-induced fibrotic livers.

Prediction of differentially expressed circRNA-related target genes and construction of circRNA/miRNA/mRNA networks. The identification of circRNA target genes is crucial for characterizing circRNA function. One of the molecular functions of circRNAs is their role as a ceRNA, which regulate miRNAs and consequently modulate mRNA expression (24,49). The interactions among circRNA, miRNA and mRNA were assessed based on the differentially expressed circRNAs between PZH-treated and the CCl_4-inducted groups; the results showed that the upregulated circRNAs had interactions with 139 miRNA binding sites and 927 target genes. A total of 103 potential miRNAs binding sites and 887 target genes of these miRNAs were also identified on downregulated circRNAs (Table SV). Multiple circRNA-related biomarkers associated with liver fibrosis were also identified using circRNA-seq. However, the number of putative biomarkers was too large to accurately identify the biomarkers that may be involved in PZH treatment of liver fibrosis. Therefore, only the predicted target genes of the differentially expressed circRNAs were selected for further analysis.

The predicted set of functional genes for up- or down-regulated circRNAs was compared with a set of differentially expressed mRNA genes enriched in the mRNA-seq data (these mRNAs were enriched in the same treatment conditions as those in the present study) (GEO accession no. GSE133481). The shared genes between these two datasets were recorded. In the upregulated circRNAs, only 10 overlapping genes from the 927 predicted mRNAs and 294 upregulated mRNAs from the mRNA-seq data were identified. Subsequently, the circRNA/miRNA/mRNA regulatory network of these related miRNAs and the corresponding significantly upregulated

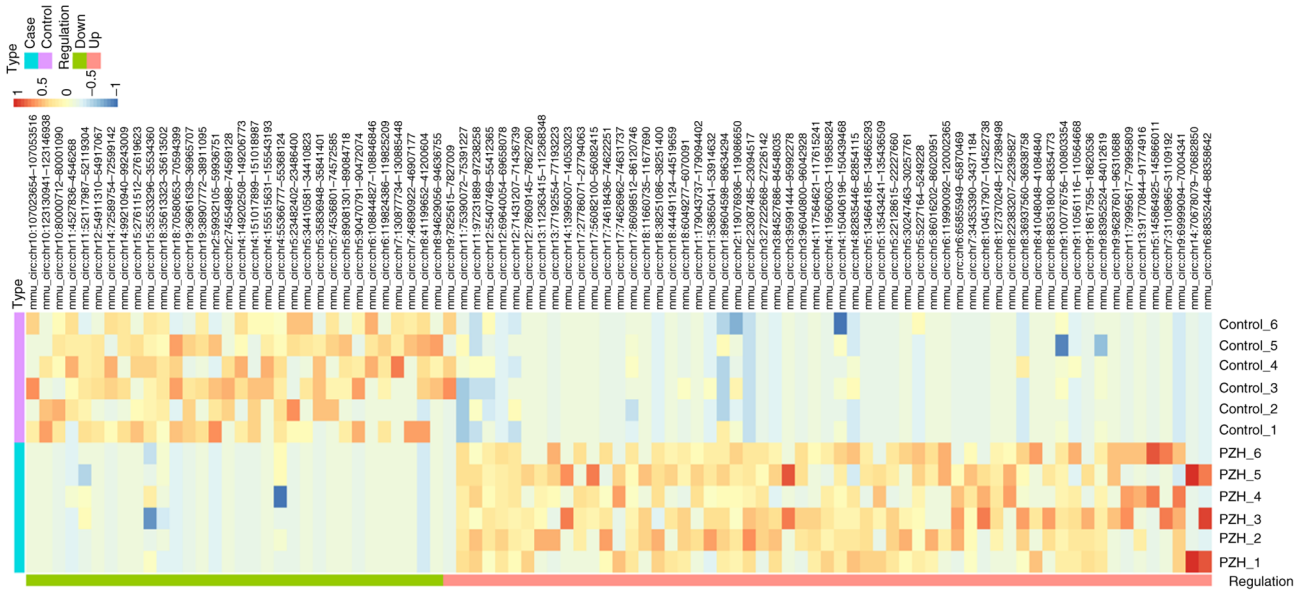

Figure 3. CCl_4-induced and PZH-treated mouse models of liver fibrosis. Hierarchical clustering of differentially expressed circRNAs between the two groups (n=6 mice/group). Each column represents the indicated circRNA; each row represents one sample. Red indicates high expression levels; blue indicates low expression levels. CCl_4, carbon tetrachloride; chr, chromosome; circRNA, circular RNA; mmu, *Mus musculus*; PZH, Pien Tze Huang.

circRNA-binding sites were constructed (Fig. 4A). The results demonstrated that 10 upregulated mRNAs were found to interact with 15 miRNAs, which were involved in the regulation of 17 circRNAs. Among the 15 miRNAs in the circRNA/miRNA/mRNA regulatory network, mmu-miR-466i-5p was targeted by seven identified upregulated circRNAs and exhibited the largest interaction network. miR-345-3p was predicted to be negatively modulated by mmu_circ:chromosome (chr)9:69999094|70004341 and mmu_circ:chr2:119076936|119086650. The following top five most upregulated circRNAs appeared to be associated with the largest binding miRNA network: mmu_circ:chr17:74626961|74631737, mmu_circ:chr2:119076936|119086650, mmu_circ:chr13:112363415|112368348, mmu_circ:chr17:27786071|27794063 and mmu_circ:chr9:69999094|70004341. In the downregulated circRNAs, 21 overlapping genes from the 887 predicted mRNAs and 558 downregulated mRNAs from the mRNA-seq data were identified. Similarly, the circRNA/miRNA/mRNA regulatory network of these related miRNAs and the corresponding significantly downregulated circRNA-binding sites were constructed (Fig. 4B). The results demonstrated that 21 downregulated mRNAs were found to interact with 27 miRNAs, which were involved in the regulation of 12 downregulated circRNAs. The following top five most downregulated circRNAs were found to be associated with the largest binding miRNA network: mmu_circ:chr12:54911310|54917067, mmu_circ:chr15:27611512|27619623, mmu_circ:chr4:149202507|149206773, mmu_circ:chr5:23482401|23486400 and mmu_circ:chr5:89081301|89084718. The expression information for the dysregulated circRNAs and their related target genes involved in circRNA/miRNA/mRNA interaction networks are listed in Tables III and IV, respectively. A flowchart summarizing the circRNA/miRNA/mRNA interaction network associated with the dysregulated circRNAs, as well as the results of the subsequent target gene analysis, is displayed in Fig. 5.

Host gene enrichment analysis of differentially expressed circRNA-related target genes. The function of all differentially expressed circRNA-related target genes was further explored. The GO analysis results demonstrated that the target genes mainly participated in the biological processes of 'positive regulation of fibroblast proliferation', 'response to endogenous stimulus', 'drug catabolic process' and 'regulation of DNA-templated transcription in response to stress' (Fig. 6A). KEGG pathways were also identified for differentially expressed circRNA-related target genes. KEGG analysis identified the following enriched pathways: 'Metabolic pathways', 'TNF signaling pathway', 'PI3K-Akt signaling pathway', 'IL-17 signaling pathway', 'MAPK signaling pathway' and 'apoptosis' ($P<0.05$; Fig. 6B). Meanwhile, the results of GO pathway analyses showed that the differentially expressed circRNA-related target genes in this network were associated with cellular components, such as 'fibrinogen complex', 'transcription factor AP-1 complex' and 'platelet alpha granule'; and molecular functions, such as 'ketosteroid monooxygenase activity' and 'MAP kinase tyrosine/serine/threonine and phosphatase activity' (Fig. S2).

Validation of candidate circRNA-related target genes by RT-qPCR. To verify the results of the co-expression network analysis, seven overlapping circRNA-related target gene candidates were selected for RT-qPCR in LX-2 cells in the CCL_4-induced and PZH-treated group (Table V). mRNA expression levels of the seven gene candidates were subsequently detected 24, 48 and 72 h following PZH treatment (0.75 mg/ml). The seven selected transcripts included: Tyrosine 3-monooxygenase/tryptophan 5-monooxygenase activation protein γ (YWHAG); solute carrier family 39, member 14 (SLC39A14); FOS-like 2, AP-1 transcription factor subunit (FOSL2); solute carrier family 7, member 11 (SLC7A11); serpin family E, member 1 (SERPINE1); ATPase sarcoplasmic/endoplasmic reticulum Ca^{2+} (ATP2A2); and NRAS

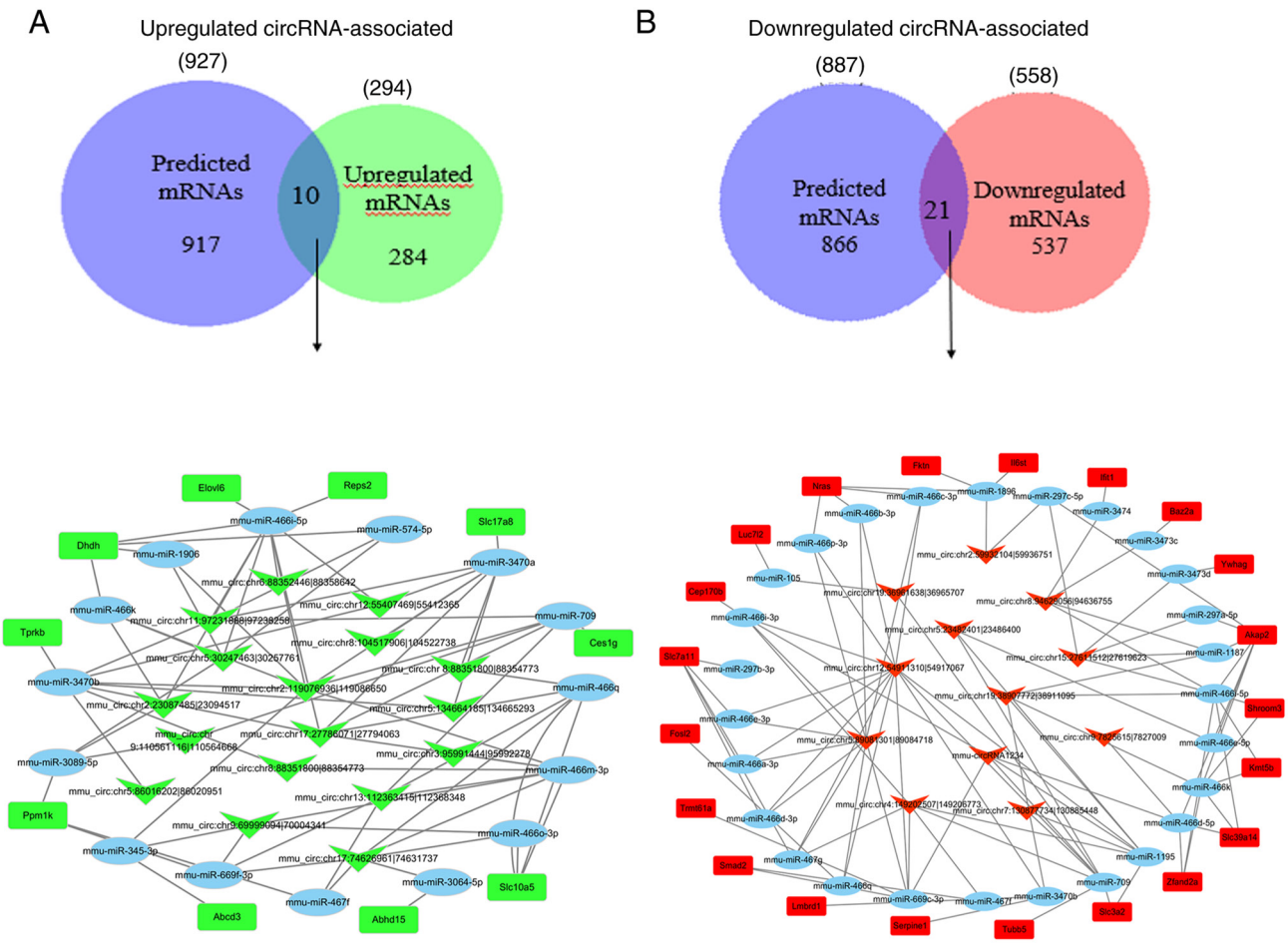

Figure 4. circRNA-seq data analysis. (A) Between the upregulated circRNA-related target genes and the upregulated genes obtained from the mRNA-seq data, 10 overlapping genes were identified. The circRNA/miRNA/mRNA regulatory network of their related miRNAs and their corresponding significantly upregulated circRNA-binding sites was constructed. The network consisted of 17 circRNAs (arrowheads), 15 miRNAs (ellipses), 10 mRNAs (rectangles) and 75 connections. (B) Between the downregulated circRNA-related target genes and the downregulated genes obtained from the mRNA-seq data 21 overlapping genes were identified. The circRNA/miRNA/mRNA regulatory network of their related miRNAs and the corresponding significantly downregulated circRNA-binding sites was constructed. The network consisted of 12 circRNAs (arrowheads), 27 miRNAs (ellipses), 21 mRNAs (rectangles) and 101 connections. Abcd3, ATP-binding cassette subfamily D, member 3; Abhd15, abhydrolase domain-containing 15; Akap2, A-kinase-anchoring protein 2; Baz2a, bromodomain adjacent to zinc-finger domain 2A; Cep170b, centrosomal protein 170B; Ces1gES1G, carboxylic ester hydrolase; chr, chromosome; circRNA, circular RNA; Dhdh, dihydrodiol dehydrogenase; Fktn, fukutin; Fosl2, FOS-like 2, AP-1 transcription factor subunit; Ifit1, interferon induced protein with tetratricopeptide repeats 1; Il6st, interleukin 6 cytokine family signal transducer; Kmt5b, lysine methyltransferase 5B; Lmbrd1, LMBR1 domain-containing 1; Luc7l2, putative RNA-binding protein Luc7-like 2; miR, microRNA; seq, sequencing; mmu, *Mus musculus*; Nras, NRAS proto-oncogene GTPase; Ppm1k, protein phosphatase Mg^{2+}/Mn^{2+} dependent 1K; Serpine1, serpin family E, member 1; Shroom3, shroom family member 3; Slc3a2, solute carrier family 3, member 2; Slc7a11, solute carrier family 7, member 11; Slc10a5, solute carrier family 10, member 5; Slc17a8, solute carrier family 17, member 8; Slc39a14, solute carrier family 39, member 14; Tprkb, TP53RK binding protein; TRMT61A, tRNA methyltransferase 61A; Tubb5, tubulin b class I; Ywhag, tyrosine 3-monooxygenase/tryptophan 5-monooxygenase activation protein g; Zfand2a, zinc-finger AN1-type-containing 2A Smad2, SMAD family member 2; Trmt61a, tRNA methyltransferase 61A; Reps2, RALBP1-associated Eps domain-containing 2; Elovl6, ELOVL fatty acid elongase 6.

proto-oncogene GTPase (NRAS). Among these seven, seven (SLC39A14, FOSL2, SLC7A11, SERPINE1, ATP2A2 and NRAS) were significantly differentially expressed compared with the control (Fig. 7). SLC39A14, FOSL2, SLC7A11, SERPINE1, ATP2A2 and NRAS mRNA expression levels were significantly downregulated in the PZH-treated group compared with the control group, while YWHAG was significantly upregulated. Overall, the results of the RT-qPCR validation of overlapping candidate circRNA-related target genes were consistent with the mRNA-seq results.

Survival analysis between patient mortality and differentially expressed circRNA-related target gene expression levels in liver hepatocellular carcinoma (LIHC). To explore the relationship between the expression levels of overlapping functional genes associated with differentially expressed circRNAs and patient survival, 269 patients with LIHC from TCGA database were divided into low- and high-expression groups based on the median values. The mRNA expression of 2 out of the 31 overlapping functional genes was significantly associated with patient survival in LIHC (Fig. 8). These were dihydrodiol dehydrogenase (DHDH) and SLC7A11. Kaplan-Meier survival analysis demonstrated that patients with low DHDH expression levels exhibited a greater survival rate compared with those with high DHDH expression levels (log-rank test, P=0.0057; Fig. 8A). The results for DHDH were also consistent with the survival rate of patients with LIHC based on SLC7A11 mRNA expression analysis (log-rank test,

Table III. Information on identified dysregulated circRNAs.

circRNA ID	Gene	Log_2 fold-change	Regulation	P-value
mmu_circ:chr9:69999094|70004341	Bnip2	2.669154139	Up	$3.41x10^{-7}$
mmu_circ:chr3:95991444|95992278	Plekho1	1.817786326	Up	$1.82x10^{-2}$
mmu_circ:chr2:119076936|119086650	Knl1	1.020291023	Up	$4.89x10^{-2}$
mmu_circ:chr2:23087485|23094517	Acbd5	2.518912306	Up	$4.36x10^{-9}$
mmu_circ:chr6:88352446|88358642	Eefsec	2.828790508	Up	$5.39x10^{-5}$
mmu_circ:chr11:97231888|97238258	Npepps	1.851337918	Up	$1.47x10^{-2}$
mmu_circ:chr5:30247463|30257761	Selenoi	1.219232659	Up	$2.83x10^{-2}$
mmu_circ:chr17:27786071|27794063	D17Wsu92e	1.065565101	Up	$3.40x10^{-2}$
mmu_circ:chr12:55407469|55412365	Psma6	1.056995708	Up	$4.91x10^{-2}$
mmu_circ:chr5:134664185|134665293	Limk1	1.514958004	Up	$1.56x10^{-3}$
mmu_circ:chr8:104517906|104522738	Nae1	1.699428017	Up	$9.48x10^{-3}$
mmu_circ:chr8:88351800|88354773	Brd7	1.258290693	Up	$4.82x10^{-2}$
mmu_circ:chr17:74626961|74631737	Birc6	1.408138487	Up	$1.64x10^{-2}$
mmu_circ:chr13:112363415|112368348	Ankrd55	1.086885064	Up	$3.34x10^{-2}$
mmu_circ:chr9:110561116|110564668	Setd2	1.583016549	Up	$4.16x10^{-2}$
mmu_circ:chr5:86016202|86020951	Cenpc1	1.286666981	Up	$2.53x10^{-2}$
mmu_circ:chr8:88351800|88354773	Brd7	1.258290693	Up	$4.82x10^{-2}$
mmu_circ:chr5:89081301|89084718	Slc4a4	-1.033058375	Down	$4.03x10^{-2}$
mmu_circ:chr12:54911310|54917067	Baz1a	-1.044583375	Down	$4.22x10^{-2}$
mmu_circ:chr2:59932104|59936751	Baz2b	-1.850754348	Down	$1.53x10^{-3}$
mmu_circ:chr8:94629056|94636755	Rspry1	-1.304377354	Down	$4.43x10^{-2}$
mmu_circ:chr19:36961638|36965707	Btaf1	-1.363049915	Down	$1.51x10^{-2}$
mmu_circ:chr15:27611512|27619623	Otulin	-1.229226523	Down	$1.72x10^{-2}$
mmu_circ:chr19:38907772|38911095	Tbc1d12	-1.144664409	Down	$2.61x10^{-2}$
mmu-circRNA1234	Fndc3a	-1.384170351	Down	$1.41x10^{-2}$
mmu_circ:chr9:7825615|7827009	Birc2	-1.539082966	Down	$2.21x10^{-2}$
mmu_circ:chr4:149202507|149206773	Kif1b	-1.503481469	Down	$2.16x10^{-3}$
mmu_circ:chr5:23482401|23486400	Kmt2e	-1.397731511	Down	$5.86x10^{-3}$
mmu_circ:chr7:130877734|130885448	Plekha1	-1.335857428	Down	$3.53x10^{-2}$

chr, chromosome; circRNA/circ, circular RNA; mmu, *Mus musculus*.

P=0.017; and Fig. 8B). However, Kaplan-Meier survival analysis of the remaining genes, including RALBP1-associated Eps domain-containing 2 (REPS2), SERPINE1, solute carrier family 3, member 2 (SLC3A2) and solute carrier family 10, member 5 (SLC10A5), indicated that although the difference in LIPC survival rates between high-expression and low-expression groups was not statistically significant (log-rank test, P=0.07, P=0.21, P=0.22 and P=0.33, respectively), the mRNA expression levels of these genes were still closely associated with the survival of the patients (Fig. 8C-F).

Discussion

Traditional Chinese Medicine PZH has attracted considerable attention due to its marked therapeutic effect on liver injury (15,16). PZH exposure has been reported to significantly reduce cell necrosis and swelling, microvesicular steatosis and lymphocyte infiltration in the injured liver (50). Previous studies have shown that PZH may affect the immune system by interfering with the expression of functional genes in immune-related pathways in CCl_4-induced mice (15,50). CCl_4 is the mostly used reagent for the induction of liver injury animal models. Our previous study demonstrated that the ratio of positive Sirius red staining against the total area was significantly decreased in the PZH treatment group compared with the non-treatment group using Sirius red staining (39). These results prompted us to explore potential molecular mechanisms underlying these observed effects in a PZH-treated CCl_4-induced liver injury model. circRNAs have certain advantages in the development and application of new clinical diagnostic markers, for example, Ye *et al* found that circRNAs participate in the pathogenesis of hepatic injury and providing efficient targets in the therapy against liver injury (28), and increasing number of studies have reported that circRNAs may act as miRNA sponges to regulate disease occurrence and development (21,24,49). However, to the best of our knowledge, there are currently no studies on the regulatory mechanisms of differentially expressed circRNAs in PZH-treated liver damage using RNA-seq technology. Therefore, mining circRNA transcript expression profiles using RNA-seq is

Table IV. Overlapping genes between dysregulated circular RNA-associated target genes and differentially expressed mRNAs.

Gene	Log_2 fold-change	Regulation	P-value	Full name
Abcd3	1.0280	Up	$7.92x10^{-6}$	ATP-binding cassette subfamily D, member 3
Elovl6	1.1377	Up	$2.83x10^{-4}$	ELOVL fatty acid elongase 6
Slc17a8	1.2805	Up	$2.05x10^{-6}$	Solute carrier family 17, member 8
Ppm1k	1.0442	Up	$4.30x10^{-4}$	Protein phosphatase, Mg^{2+}/Mn^{2+} dependent 1K
Tprkb	1.3508	Up	$2.78x10^{-2}$	TP53RK-binding protein
Slc10a5	1.6327	Up	$1.58x10^{-6}$	Solute carrier family 10, member 5
Reps2	1.1568	Up	$2.75x10^{-2}$	RALBP1-associated Eps domain-containing 2
Ces1g	1.2722	Up	$6.21x10^{-5}$	Carboxylesterase 1G
Dhdh	1.4262	Up	$1.26x10^{-6}$	Dihydrodiol dehydrogenase
Abhd15	1.1437	Up	$6.69x10^{-5}$	Abhydrolase domain-containing 15
Nras	-1.0682	Down	$3.79x10^{-2}$	NRAS proto-oncogene, GTPase
Baz2a	-1.1493	Down	$2.07x10^{-2}$	Bromodomain adjacent to zinc-finger domain 2A
Luc7l2	-1.2942	Down	$2.23x10^{-2}$	LUC7 like 2, pre-mRNA splicing factor
Ywhag	-1.1007	Down	$5.95x10^{-6}$	Tyrosine 3-monooxygenase/tryptophan 5-monooxygenase activation protein γ
Serpine1	-3.3643	Down	$5.52x10^{-5}$	Serpin family E, member 1
Zfand2a	-1.2588	Down	$1.21x10^{-2}$	Zinc-finger AN1-type-containing 2A
Smad2	-1.1590	Down	$3.52x10^{-3}$	SMAD family member 2
Kmt5b	-1.4307	Down	$2.56x10^{-2}$	Lysine methyltransferase 5B
Slc3a2	-1.5998	Down	$9.27x10^{-7}$	Solute carrier family 3, member 2
Trmt61a	-1.0673	Down	$1.30x10^{-4}$	tRNA methyltransferase 61A
Cep170b	-1.5367	Down	$7.12x10^{-3}$	Centrosomal protein 170B
Slc7a11	-2.2590	Down	$1.40x10^{-5}$	Solute carrier family 7, member 11
Il6st	-1.0635	Down	$4.03x10^{-5}$	Interleukin 6 signal transducer
Ifit1	-1.0547	Down	$4.36x10^{-3}$	Interferon-induced protein with tetratricopeptide repeats 1
Tubb5	-1.2318	Down	$9.96x10^{-7}$	Tubulin, β5 class I
Lmbrd1	-1.4803	Down	$2.68x10^{-2}$	LMBR1 domain-containing 1
Fktn	-1.0167	Down	$4.39x10^{-3}$	Fukutin
Akap2	-1.2242	Down	$1.25x10^{-3}$	A-kinase anchoring protein 2
Fosl2	-1.2528	Down	$5.73x10^{-5}$	FOS-like 2, AP-1 transcription factor subunit
Slc39a14	-1.0692	Down	$5.52x10^{-4}$	Solute carrier family 39, member 14
Shroom3	-1.2148	Down	$1.19x10^{-2}$	Shroom family member 3

Table V. Selected candidate circular RNA-associated target genes for reverse transcription-quantitative PCR.

Gene[a]	Full name	Role in liver injury	(Refs.)
Slc7a11	Solute carrier family 7, member 11	Induced in activated hepatic stellate cells	(78)
Serpine1	Serpin family E, member 1	Progression of fibrosis	(79,80)
Fosl2	FOS-like 2, AP-1 transcription factor subunit	Progression of fibrosis	(67)
Atp2a2	A-kinase anchoring protein 2	Progression of fibrosis	(81)
Nras	NRAS proto-oncogene, GTPase	Progression of hepatocellular carcinoma	(82)
Slc39a14	Solute carrier family 39, member 14	Progression of fibrosis	(83)
Ywhag	Tyrosine 3-monooxygenase/tryptophan 5-monooxygenase activation protein γ	Progression of fibrosis	(84)

[a]Genes known to serve a role in fibrosis or liver injury.

important for exploring the pathological mechanism of PZH in the treatment of liver diseases, especially liver fibrosis. In the present study, circRNA-seq and bioinformatic analyses were used to explore the function of circRNAs in PZH-treated mice

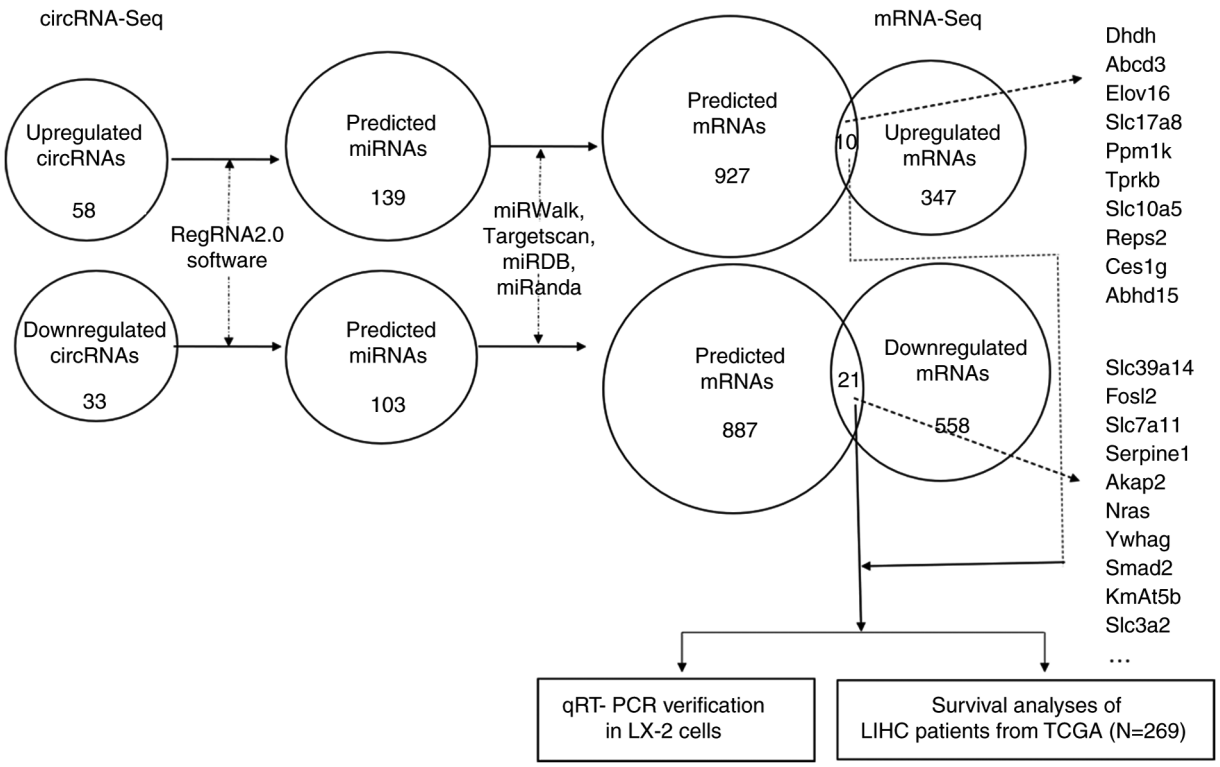

Figure 5. Bioinformatics analysis and experimental verification of up- and downregulated circRNAs between the PZH-treated and untreated control group. The shared mRNAs between the differentially expressed circRNA-related predicted target genes in the present study and the differentially expressed mRNAs from mRNA-seq data (GEO accession no. GSE133481) were extracted for further analysis. Abcd3, ATP-binding cassette subfamily D, member 3; Abhd15, abhydrolase domain-containing 15; Akap2, A-kinase-anchoring protein 2; Ces1g, carboxylic ester hydrolase; circRNA, circular RNA; Dhdh, dihydrodiol dehydrogenase; Elov16, ELOVL fatty acid elongase 6; Fosl2, FOS-like 2, AP-1 transcription factor subunit; Kmat5b, lysine methyltransferase 5B; LIHC, liver hepatocellular carcinoma; miR, microRNA; Nras, NRAS proto-oncogene GTPase; Ppm1k, protein phosphatase Mg^{2+}/Mn^{2+} dependent 1K; PZH, Pien Tze Huang; Reps2, RALBP1-associated Eps domain-containing 2; RT-qPCR, reverse transcription-quantitative PCR; Serpine1, serpin family E, member 1; seq, sequencing; Slc3a2, solute carrier family 3, member 2; Slc7a11, solute carrier family 7, member 11; Slc10a5, solute carrier family, 10 member 5; Slc17a8, solute carrier family 17, member 8; Slc39a14, solute carrier family 39, member 14; TCGA, The Cancer Genome Atlas; Tprkb, TP53RK-binding protein; Ywhag, tyrosine 3-monooxygenase/tryptophan 5-monooxygenase activation protein γ.

with liver fibrosis. The circRNA expression profile identified 91 differentially expressed circRNAs between the PZH-treated and CCl_4-induced groups, of which 58 were upregulated and 33 were downregulated. To the best of our knowledge this was the first study to provide evidence that circRNAs are differentially expressed in PZH-treated fibrotic liver tissue compared with the controls, which used CCl_4 only.

CircRNAs act as miRNA sponges that regulate target gene expression by binding to miRNAs (24). The present study predicted that there were 242 miRNA-binding sites on circRNAs and 994 differentially expressed circRNA-related target genes using related software, and these results were similar to previous reports in human studies (26,27,29). To gain insights into the function of differentially expressed circRNAs, GO term and KEGG pathway enrichment analyses were performed. From the KEGG pathway enrichment analysis, it was determined that all differentially expressed circRNA-related target genes were found to be involved in several crucial pathways, including 'metabolic pathways', 'TNF signaling pathway', 'PI3K-Akt signaling pathway', 'IL-17 signaling pathway', 'MAPK signaling pathway' and 'apoptosis'. Previous studies have reported that the PI3K/Akt signaling pathway is important for HSC activation and apoptosis, as well as the regulation of proliferation in liver fibrosis (51-53). Shu *et al* (54) demonstrated that the inhibition of the MAPK signaling pathway alleviates CCl_4-induced liver fibrosis in Toll-like receptor 5-deficient mice. Furthermore, Ghallab *et al* (55) identified that the TGF-β and TNF-α inflammatory pathways were activated by influencing lobular zonation of liver fibrosis. Moreover, the activation of the IL-17 signaling pathway may inhibit the development of liver fibrosis (56,57). It can therefore be hypothesized that the differential expression of circRNAs in these signaling pathways serves an important role in PZH-induced improvement in the fibrotic liver.

In the present study, a co-expression network was constructed based on the circRNA-seq and mRNA-seq data to investigate their interactions. The predicted set of functional genes for up- or downregulated circRNAs overlapped with a set of differentially expressed mRNA genes. In the upregulated circRNAs, 10 overlapping genes were identified and the circRNA/miRNA/mRNA regulatory network of 15 related miRNAs and a corresponding 17 significantly upregulated circRNA-binding sites on these miRNAs was constructed. Hyun *et al* (58) demonstrated that miR-466i-5p was significantly upregulated in the CCl_4-induced liver fibrosis model group, which further aggravated the activation of HSCs and induced liver fibrosis. Another report suggested that ELOVL fatty acid elongase 6 (ELOV16) expression was significantly downregulated in human lungs with idiopathic pulmonary fibrosis (59). The results of the present study indicated that

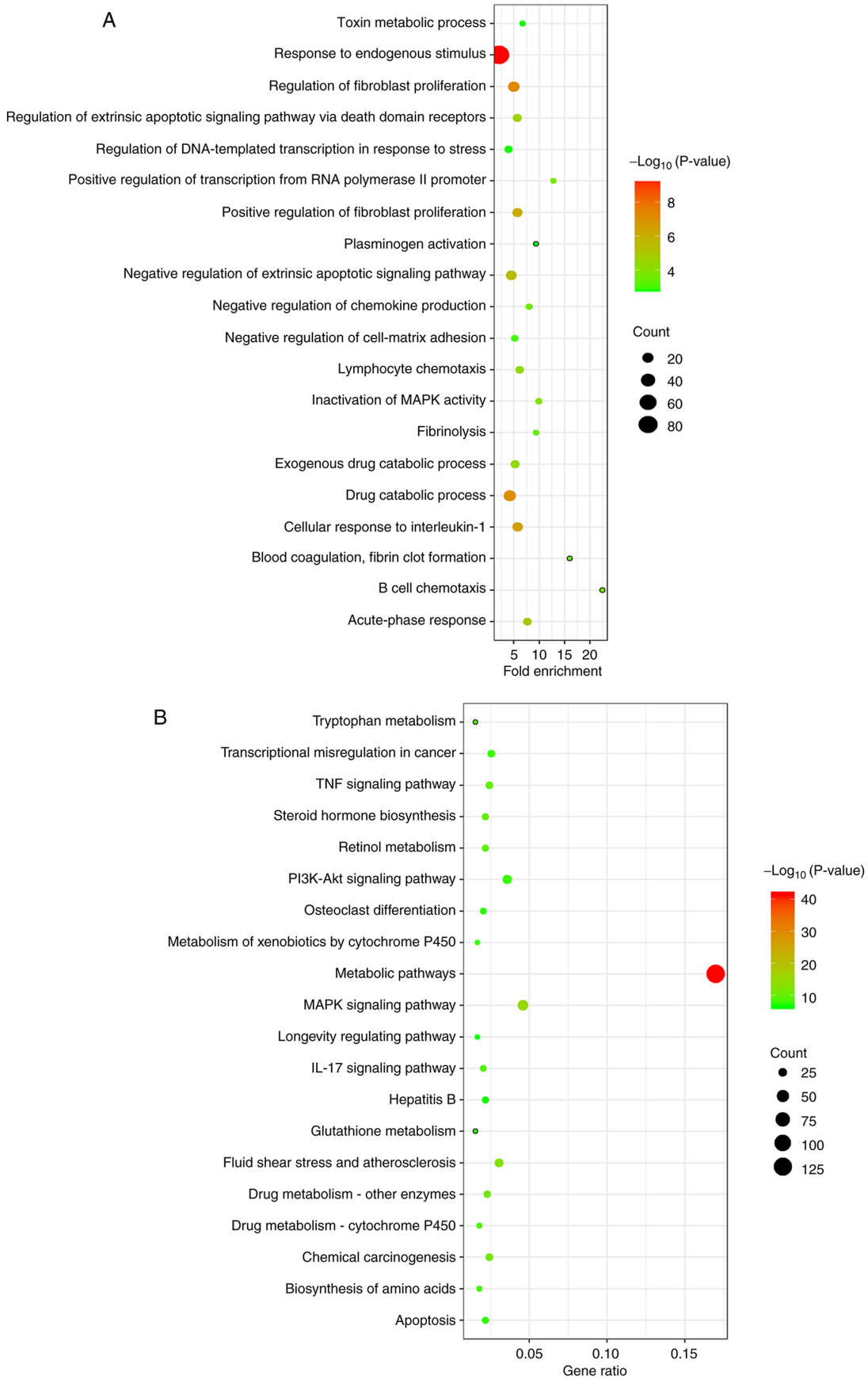

Figure 6. GO term annotation and KEGG pathway enrichment analyses of differentially expressed circRNA-related target genes. (A) Biological process GO terms corresponding to the differentially expressed circRNAs. (B) KEGG enriched pathways for the target genes of the differentially expressed circRNAs. The x-axes indicate fold enrichment and the ratio of enriched differentially expressed genes in each pathway. The y-axes denote the name of the enriched KEGG pathway. The area of each node represents the number of enriched differentially expressed genes. The -$\log_{10}$(P-value) was visualized using a green to red color variation bar. P<0.05 was considered to indicate a statistically significant difference. circRNAs, circular RNAs; GO, Gene Ontology; KEGG, Kyoto Encyclopedia of Genes and Genomes.

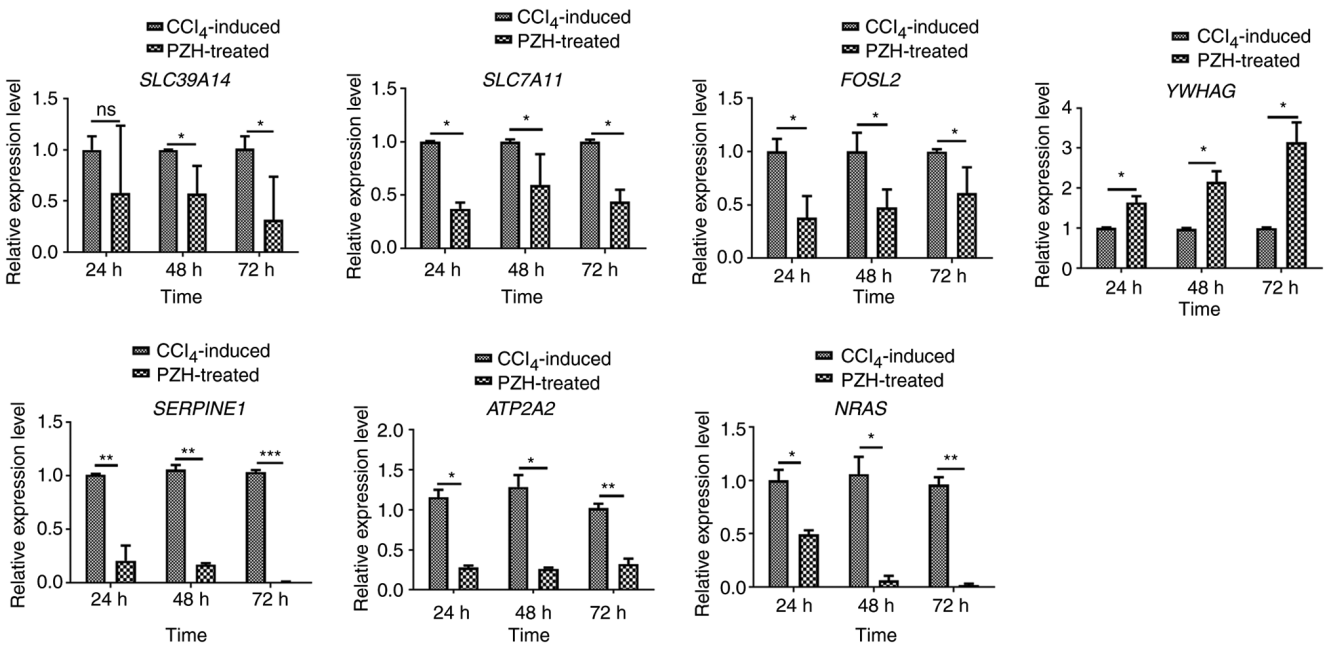

Figure 7. Validation of target genes displayed in competing endogenous RNA networks in LX-2 cells by reverse transcription-quantitative PCR. Data are presented as the median ± SEM. *P<0.05, **P<0.01 and ***P<0.001. ATP2A2, ATPase sarcoplasmic/endoplasmic reticulum Ca^{2+}; FOSL2, FOS-like 2, AP-1 transcription factor subunit; NRAS, NRAS proto-oncogene GTPase; PZH, Pien Tze Huang; SERPINE1, serpin family E, member 1; SLC7A11, solute carrier family 7, member 11; SLC39A14, solute carrier family 39, member 14.

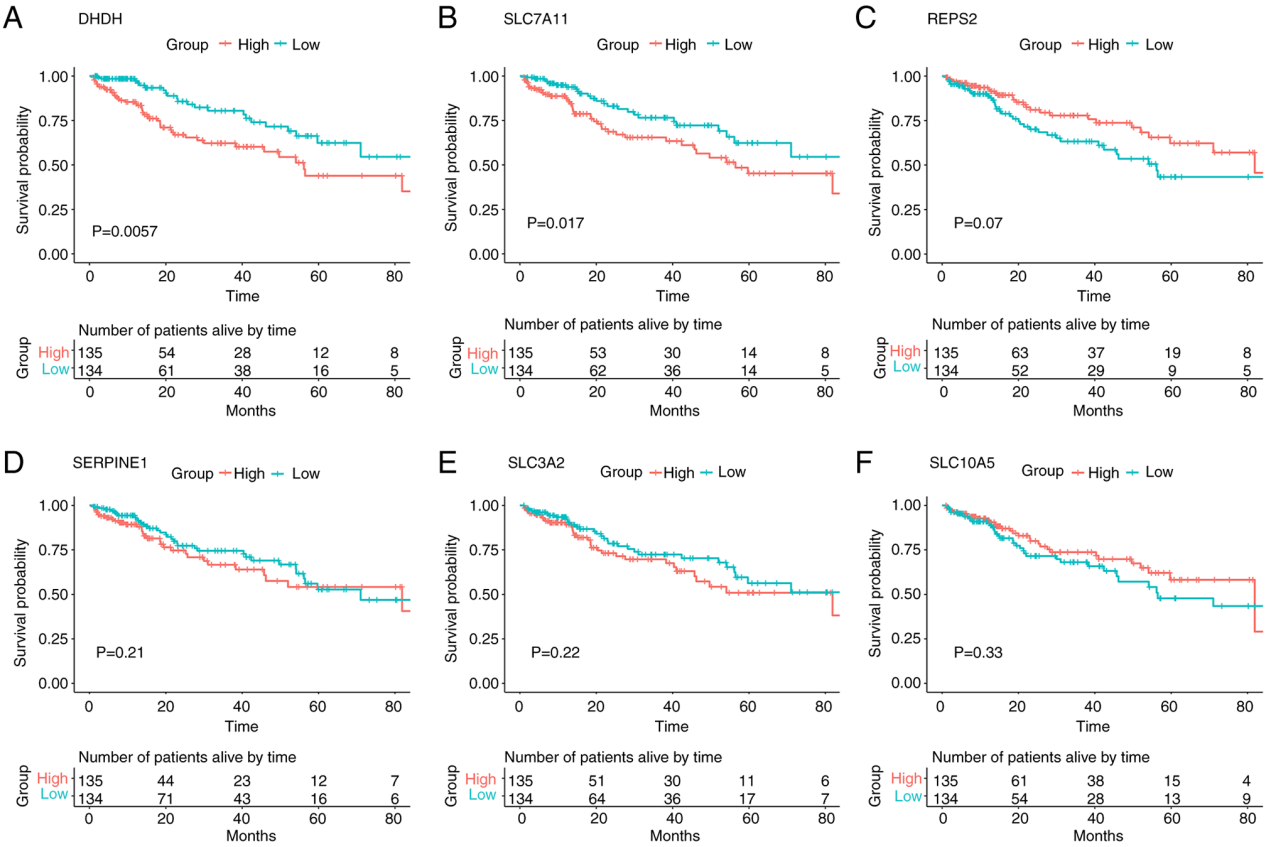

Figure 8. Kaplan-Meier survival analysis between the patient clinical outcomes and circular RNA-related target genes. (A) DHDH, (B) SLC7A11, (C) REPS2, (D) SERPINE1, (E) SLC3A2 and (F) SLC10A5 gene expression levels in 269 patients with liver hepatocellular carcinoma from The Cancer Genome Atlas cohort were used to plot survival curves produced using Kaplan-Meier survival analysis. Patients exhibiting gene expression levels higher than the median values were assigned to the high-expression group, whereas those exhibiting mRNA expression levels lower than the median values were assigned to the low-expression group. The log-rank test was used to compare the difference in survival rates between the high- and low-mRNA expression groups. P<0.05 was considered to indicate a statistically significant difference. DHDH, dihydrodiol dehydrogenase; REPS2, RALBP1-associated Eps domain-containing 2; SLC3A2, solute carrier family 3, member 2; SLC7A11, solute carrier family 7, member 11; SLC10A5, solute carrier family 10, member 5; SERPINE1, serpin family E, member 1.

seven of the identified upregulated circRNAs may serve an important role in the therapeutic effect of PZH in the fibrotic liver by decreasing the expression levels of miR-466i-5p and further increasing those of ELOV16. Previous studies have also reported that miR-345-3p upregulation is involved in the pathogenesis of liver fibrosis and hepatocellular carcinoma (HCC) by negatively regulating cyclin-dependent kinase inhibitor 1 in cancer cells (57,60). This result indicated that the overexpression of these two circRNAs may induce pulmonary fibrosis by decreasing miR-345-3p expression levels and consequently increasing that of ATP-binding cassette subfamily D, member 3. In the downregulated circRNAs, 21 overlapping genes were identified and the circRNA/miRNA/mRNA regulatory network of 27 related miRNAs and the corresponding 12 significantly downregulated circRNA-binding sites on these miRNAs was constructed. A previous study reported that miRNA-105 expression is markedly downregulated in both HCC cell lines and clinical HCC tissues, compared with normal human hepatocyte and adjacent non-cancerous tissues (61). The results of the present study found 12 significantly downregulated circRNA-binding sites in PZH-treated fibrotic livers in model mice. An *et al* (62) demonstrated that miR-467f is downregulated in acute liver failure compared with mock-treated livers. Furthermore, the increased expression of SMAD2 has been demonstrated to serve a vital role in the development of liver fibrosis (63). The results of the present study indicated that downregulated mmu_circ:chr4:149202507|149206773 may participate in the therapeutic effects of PZH on the fibrotic liver by decreasing the expression of SMAD2. Overall, these results demonstrated that differentially expressed circRNAs may alter the expression of certain functional genes via the circRNA/miRNA/mRNA regulatory network, therefore mediating PZH-treated liver fibrosis. It was therefore hypothesized that differentially expressed circRNAs may act as miRNA sponges and serve an important role in PZH-treated liver fibrosis by preventing miRNAs from regulating their target mRNAs.

The RT-qPCR data for the six differentially expressed circRNA-related target genes in the LX-2 cell model were consistent with the trends observed in the mRNA-seq data. Among the verified genes, SLC7A11 was the one most widely investigated in liver damage. It has previously been reported that inhibiting SLC7A11 induces ferroptosis in myofibroblastic HSCs and protects against liver fibrosis (64). Zhang *et al* (65) reported that the upregulation of SLC7A11 is an indicator of unfavorable prognosis in liver carcinoma. Furthermore, SERPINE1 has been demonstrated to serve an important role in the development of liver fibrosis. Lodder *et al* (66) found that increased expression of gene SERPINE1 aggravating the degree of liver fibrosis, liver cell damage and inflammation in myeloid cells. A previous study also demonstrated that homolog Fos-related antigen 2, encoded by FOSL2, is a contributing pathogenic factor of pulmonary fibrosis in humans (67). Furthermore, NRAS is a proto-oncogene, whose activating mutation has been linked to several types of human cancer, including HCC (68,69). Previous studies have demonstrated that sustained NRAS activation resulting from the overexpression of constitutively active NRAS, induces HCC in genetically compromised mice (70,71). In the present study, the results of the RT-qPCR validation of the differentially expressed circRNA-related target genes (SLC7A11, SERPINE1, FOSL2, NRAS, SLC39A14 and ATP2A2) corresponded to the mRNA-seq results. These results further suggested that the differentially expressed circRNAs acted as miRNA sponges in the regulation of target gene expression to influence the effects of PZH-treatment on liver fibrosis.

To explore the association between the differentially expressed circRNA-related targets and the survival time of patients with LIHC, Kaplan-Meier survival analysis was performed using data from the TCGA (n=269). The upregulated genes in PZH-treated liver fibrosis (SLC7A11 and DHDH) were found to be significantly positively associated with patient survival. Yue *et al* (72) reported that SLC7A11 served an important role in HCC as a potential prognostic indicator and its overexpression promoted HCC development. Furthermore, SLC7A11 may be a prognostic factor for liver carcinoma, as indicated by the survival analysis (73). Elevated levels of plasminogen activator inhibitor-1 (the protein product of SERPINE1) have been reported in patients with viral infection-related HCC (74). A number of studies have also indicated that SERPINE1 may contribute to cancer dissemination mechanisms, including the prevention of excessive ECM degradation, modulation of cell adhesion and stimulation of angiogenesis and cell proliferation (75,76). Wu *et al* (77) reported that SLC3A2 was highly expressed in the human HCC cell membrane and may serve an important role in promoting tumor metastasis and HCC progression. Overall, these results indicated that a specific set of differentially expressed circRNA-related functional genes may act as therapeutic targets for liver injury.

In conclusion, the present study identified 91 differentially expressed circRNAs in a PZH-treated CCl_4-induced liver fibrosis model and the potential functions of 6 circRNA-related target genes were validated in LX-2 cells. Kaplan-Meier survival analysis further confirmed that two target mRNAs had potential clinical prognostic value for LIHC. Meanwhile, a functional circRNA/miRNA/mRNA network was systematically established to further investigate the underlying mechanisms of action of differentially expressed circRNAs. Overall, the present study provided new insights into the mechanisms underlying the pathogenesis of liver fibrosis and may provide novel and potentially efficient therapeutic targets against liver injury. However, a limitation of the present study was that it did not include any further molecular biology experiments to validate each of the differentially expressed circRNAs, and thus this will be investigated future studies.

Acknowledgements

Not applicable.

Funding

This work was supported by grants from The 863 Program (grant nos. 2012AA02A515 and 2012AA021802), The National Nature Science Foundation of China (grant nos. 81773818, 81273596, 30900799 and 81671326), The National Key Research and Development Program (grant nos. 2017YFC0909303, 2016YFC0905000, 2016YFC0905002, 2016YFC1200200 and 2016YFC0906400), The 4th Three-year Action Plan for Public

Health of Shanghai (grant no. 15GWZK0101), The Shanghai Pujiang Program (grant no. 17PJD020), The Shanghai Key Laboratory of Psychotic Disorders (grant no. 13dz2260500), The Natural Science Foundation of Fujian Province (grant no. 2016J05210), The Anhui Medical University for Scientific Research (grant no. XJ201607) and The Anhui Medical University for Scientific Research (grant no. 2017xkj006).

Availability of data and materials

The datasets generated and/or analyzed during the current study are available in the NCBI Gene Expression Omnibus repository, https://www.ncbi.nlm.nih.gov/geo/query/acc.cgi?acc=GSE150883 (accession no. GSE150883).

Authors' contributions

SQ, FH, LH and JZ designed the study. TW, JZ, DZ, HW, LC, QX, NZ, YW and LG performed the experiments. TW, LG, JM, MW and LL performed the data analysis. TW and JZ drafted the manuscript. All authors have read and approved the final manuscript. TW and JZ confirm the authenticity of all the raw data.

Ethics approval and consent to participate

The mice used in the study were obtained from the Shanghai Southern Model Animal Center. All experimental procedures were performed in accordance with the guidelines for the Care and Use of Laboratory Animals at the Chinese Academy of Animal Sciences. All animal experiments were approved by the Institutional Review Board of Shanghai Jiao Tong University (Shanghai, China; approval no. IACUC.NO:2017-0033).

Patient consent for publication

Not applicable.

Competing interests

The TCM Pien Tze Huang (PZH) was manufactured by Zhangzhhou Pien Tze Huang Pharmaceutical Co., Ltd., to which LG and FH are affiliated as employees. All other authors declare that they have no competing interests.

References

1. Mederacke I, Hsu CC, Troeger JS, Huebener P, Mu X, Dapito DH, Pradere JP and Schwabe RF: Fate tracing reveals hepatic stellate cells as dominant contributors to liver fibrosis independent of its aetiology. Nat Commun 4: 2823, 2013.
2. Schuppan D and Afdhal NH: Liver cirrhosis. Lancet 371: 838-851, 2008.
3. Shrestha N, Chand L, Han MK, Lee SO, Kim CY and Jeong YJ: Glutamine inhibits CCl4 induced liver fibrosis in mice and TGF-β1 mediated epithelial-mesenchymal transition in mouse hepatocytes. Food Chem Toxicol 93: 129-137, 2016.
4. Friedman SL: Hepatic stellate cells: Protean, multifunctional, and enigmatic cells of the liver. Physiol Rev 88: 125-172, 2008.
5. Zeisberg M and Kalluri R: Cellular mechanisms of tissue fibrosis. 1. Common and organ-specific mechanisms associated with tissue fibrosis. Am J Physiol Cell Physiol 304: C216-C225, 2013.
6. Wynn TA and Ramalingam TR: Mechanisms of fibrosis: Therapeutic translation for fibrotic disease. Nat Med 18: 1028-1040, 2012.
7. Mansour MF, Greish SM, El-Serafi AT, Abdelall H and El-Wazir YM: Therapeutic potential of human umbilical cord derived mesenchymal stem cells on rat model of liver fibrosis. Am J Stem Cells 8: 7-18, 2019.
8. Uehara T, Pogribny IP and Rusyn I: The DEN and CCl4-induced mouse model of fibrosis and inflammation-associated hepatocellular carcinoma. Curr Protoc Pharmacol 66: 14.30.1-10, 2014.
9. Morio LA, Chiu H, Sprowles KA, Zhou P, Heck DE, Gordon MK and Laskin DL: Distinct roles of tumor necrosis factor-alpha and nitric oxide in acute liver injury induced by carbon tetrachloride in mice. Toxicol Appl Pharmacol 172: 44-51, 2001.
10. Steinman L, Martin R, Bernard C, Conlon P and Oksenberg JR: Multiple sclerosis: Deeper understanding of its pathogenesis reveals new targets for therapy. Annu Rev Neurosci 25: 491-505, 2002.
11. Watanabe Y, Tsuchiya A, Seino S, Kawata Y, Kojima Y, Ikarashi S, Starkey Lewis PJ, Lu WY, Kikuta J, Kawai H, *et al*: Mesenchymal stem cells and induced bone marrow-derived macrophages synergistically improve liver fibrosis in mice. Stem Cells Transl Med 8: 271-284, 2019.
12. Altamirano-Barrera A, Barranco-Fragoso B and Méndez-Sánchez N: Management strategies for liver fibrosis. Ann Hepatol 16: 48-56, 2017.
13. Bozic M and Molleston J: Strategies for management of pediatric cystic fibrosis liver disease. Clin Liver Dis (Hoboken) 2: 204-206, 2013.
14. Chen X, Zhou H, Liu YB, Wang JF, Li H, Ung CY, Han LY, Cao ZW and Chen YZ: Database of traditional Chinese medicine and its application to studies of mechanism and to prescription validation. Br J Pharmacol 149: 1092-1103, 2006.
15. Zhao J, Zhang Y, Wan Y, Hu H and Hong Z: Pien Tze Huang Gan Bao attenuates carbon tetrachloride-induced hepatocyte apoptosis in rats, associated with suppression of p53 activation and oxidative stress. Mol Med Rep 16: 2611-2619, 2017.
16. Yang Y, Chen Z, Deng L, Yu J, Wang K, Zhang X, Ji G and Li F: Pien Tze Huang ameliorates liver injury by inhibiting the PERK/eIF2α signaling pathway in alcohol and high-fat diet rats. Acta Histochem 120: 578-585, 2018.
17. Lin W, Zhuang Q, Zheng L, Cao Z, Shen A, Li Q, Fu C, Feng J and Peng J: Pien Tze Huang inhibits liver metastasis by targeting TGF-β signaling in an orthotopic model of colorectal cancer. Oncol Rep 33: 1922-1928, 2015.
18. Lin YC, Chen YC, Chen TH, Chen HH and Tsai WJ: Acute kidney injury associated with hepato-protective Chinese Herb-Pien Tze Huang. J Exp Clin Med 3: 184-186, 2011.
19. Ragan C, Goodall GJ, Shirokikh NE and Preiss T: Insights into the biogenesis and potential functions of exonic circular RNA. Sci Rep 9: 2048, 2019.
20. Koh W, Pan W, Gawad C, Fan HC, Kerchner GA, Wyss-Coray T, Blumenfeld YJ, El-Sayed YY and Quake SR: Noninvasive in vivo monitoring of tissue-specific global gene expression in humans. Proc Natl Acad Sci USA 111: 7361-7366, 2014.
21. Hansen TB, Jensen TI, Clausen BH, Bramsen JB, Finsen B, Damgaard CK and Kjems J: Natural RNA circles function as efficient microRNA sponges. Nature 495: 384-388, 2013.
22. Zheng Q, Bao C, Guo W, Li S, Chen J, Chen B, Luo Y, Lyu D, Li Y, Shi G, *et al*: Circular RNA profiling reveals an abundant circHIPK3 that regulates cell growth by sponging multiple miRNAs. Nat Commun 7: 11215, 2016.
23. Liu YC, Li JR, Sun CH, Andrews E, Chao RF, Lin FM, Weng SL, Hsu SD, Huang CC, Cheng C, *et al*: CircNet: A database of circular RNAs derived from transcriptome sequencing data. Nucleic Acids Res 44D: D209-D215, 2016.
24. Memczak S, Jens M, Elefsinioti A, Torti F, Krueger J, Rybak A, Maier L, Mackowiak SD, Gregersen LH, Munschauer M, *et al*: Circular RNAs are a large class of animal RNAs with regulatory potency. Nature 495: 333-338, 2013.
25. Li Y, Zheng Q, Bao C, Li S, Guo W, Zhao J, Chen D, Gu J, He X and Huang S: Circular RNA is enriched and stable in exosomes: A promising biomarker for cancer diagnosis. Cell Res 25: 981-984, 2015.
26. Liang J, Wu X, Sun S, Chen P, Liang X, Wang J, Ruan J, Zhang S and Zhang X: Circular RNA expression profile analysis of severe acne by RNA-Seq and bioinformatics. J Eur Acad Dermatol Venereol 32: 1986-1992, 2018.
27. Lu C, Shi X, Wang AY, Tao Y, Wang Z, Huang C, Qiao Y, Hu H and Liu L: RNA-Seq profiling of circular RNAs in human laryngeal squamous cell carcinomas. Mol Cancer 17: 86, 2018.
28. Ye Z, Kong Q, Han J, Deng J, Wu M and Deng H: Circular RNAs are differentially expressed in liver ischemia/reperfusion injury model. J Cell Biochem 119: 7397-7405, 2018.

29. Xu H, Wang C, Song H, Xu Y and Ji G: RNA-seq profiling of circular RNAs in human colorectal cancer liver metastasis and the potential biomarkers. Mol Cancer 18: 8, 2019.
30. Bu Q, Long H, Shao X, Gu H, Kong J, Luo L, Liu B, Guo W, Wang H, Tian J, *et al*: Cocaine induces differential circular RNA expression in striatum. Transl Psychiatry 9: 199, 2019.
31. Ma X, Zhou Y, Qiao B, Jiang S, Shen Q, Han Y, Liu A, Chen X, Wei L, Zhou L and Zhao J: Androgen aggravates liver fibrosis by activation of NLRP3 inflammasome in CCl4-induced liver injury mouse model. Am J Physiol Endocrinol Metab 318: E817-E829, 2020.
32. Schroeder A, Mueller O, Stocker S, Salowsky R, Leiber M, Gassmann M, Lightfoot S, Menzel W, Granzow M and Ragg T: The RIN: An RNA integrity number for assigning integrity values to RNA measurements. BMC Mol Biol 7: 3, 2006.
33. Brown J, Pirrung M and McCue LA: FQC dashboard: Integrates FastQC results into a web-based, interactive, and extensible FASTQ quality control tool. Bioinformatics 33: 3137-3139, 2017.
34. Utturkar S, Dassanayake A, Nagaraju S and Brown SD: Bacterial differential expression analysis methods. Methods Mol Biol 2096: 89-112, 2020.
35. Dobin A and Gingeras TR: Optimizing RNA-seq mapping with STAR. Methods Mol Biol 1415: 245-262, 2016.
36. Gao Y, Wang J and Zhao F: CIRI: An efficient and unbiased algorithm for de novo circular RNA identification. Genome Biol 16: 4, 2015.
37. Zhang XO, Dong R, Zhang Y, Zhang JL, Luo Z, Zhang J, Chen LL and Yang L: Diverse alternative back-splicing and alternative splicing landscape of circular RNAs. Genome Res 26: 1277-1287, 2016.
38. Glažar P, Papavasileiou P and Rajewsky N: circBase: A database for circular RNAs. RNA 20: 1666-1670, 2014.
39. Zhu J, Zhang D, Wang T, Chen Z, Chen L, Wu H, Huai C, Sun J, Zhang N, Wei M, *et al*: Target identification of hepatic fibrosis using Pien Tze Huang based on mRNA and lncRNA. Sci Rep 11: 16980, 2021.
40. Chang TH, Huang HY, Hsu JB, Weng SL, Horng JT and Huang HD: An enhanced computational platform for investigating the roles of regulatory RNA and for identifying functional RNA motifs. BMC Bioinformatics 14 (Suppl 2): S4, 2013.
41. Dweep H, Sticht C, Pandey P and Gretz N: miRWalk-database: Prediction of possible miRNA binding sites by 'walking' the genes of three genomes. J Biomed Inform 44: 839-847, 2011.
42. Agarwal V, Bell GW, Nam JW and Bartel DP: Predicting effective microRNA target sites in mammalian mRNAs. Elife 4: e05005, 2015.
43. Dweep H and Gretz N: miRWalk2.0: A comprehensive atlas of microRNA-target interactions. Nat Methods 12: 697, 2015.
44. Adams JM and Cory S: The Bcl-2 apoptotic switch in cancer development and therapy. Oncogene 26: 1324-1337, 2007.
45. Yu G, Wang LG, Han Y and He QY: clusterProfiler: An R package for comparing biological themes among gene clusters. OMICS 16: 284-287, 2012.
46. Livak KJ and Schmittgen TD: Analysis of relative gene expression data using real-time quantitative PCR and the 2(-Delta Delta C(T)) method. Methods 25: 402-408, 2001.
47. Austin PC, Lee DS and Fine JP: Introduction to the analysis of survival data in the presence of competing risks. Circulation 133: 601-609, 2016.
48. International Cancer Genome Consortium, Hudson TJ, Anderson W, Artez A, Barker AD, Bell C, Bernabé RR, Bhan MK, Calvo F, Eerola I, *et al*: International network of cancer genome projects. Nature 464: 993-998, 2010.
49. Piwecka M, Glažar P, Hernandez-Miranda LR, Memczak S, Wolf SA, Rybak-Wolf A, Filipchyk A, Klironomos F, Cerda Jara CA, Fenske P, *et al*: Loss of a mammalian circular RNA locus causes miRNA deregulation and affects brain function. Science 357: eaam8526, 2017.
50. Zhao J, Hu H, Wan Y, Zhang Y, Zheng L and Hong Z: Pien Tze Huang Gan Bao ameliorates carbon tetrachloride-induced hepatic injury, oxidative stress and inflammation in rats. Exp Ther Med 13: 1820-1826, 2017.
51. Parsons CJ, Takashima M and Rippe RA: Molecular mechanisms of hepatic fibrogenesis. J Gastroenterol Hepatol 22 (Suppl 1): S79-S84, 2007.
52. Bai T, Lian LH, Wu YL, Wan Y and Nan JX: Thymoquinone attenuates liver fibrosis via PI3K and TLR4 signaling pathways in activated hepatic stellate cells. Int Immunopharmacol 15: 275-281, 2013.
53. Wang J, Chu ES, Chen HY, Man K, Go MY, Huang XR, Lan HY, Sung JJ and Yu J: MicroRNA-29b prevents liver fibrosis by attenuating hepatic stellate cell activation and inducing apoptosis through targeting PI3K/AKT pathway. Oncotarget 6: 7325-7338, 2015.
54. Shu M, Huang DD, Hung ZA, Hu XR and Zhang S: Inhibition of MAPK and NF-κB signaling pathways alleviate carbon tetrachloride (CCl4)-induced liver fibrosis in Toll-like receptor 5 (TLR5) deficiency mice. Biochem Biophys Res Commun 471: 233-239, 2016.
55. Ghallab A, Myllys M, Holland CH, Zaza A, Murad W, Hassan R, Ahmed YA, Abbas T, Abdelrahim EA, Schneider KM, *et al*: Influence of liver fibrosis on lobular zonation. Cells 8: 1556, 2019.
56. Meng F, Wang K, Aoyama T, Grivennikov SI, Paik Y, Scholten D, Cong M, Iwaisako K, Liu X, Zhang M, *et al*: Interleukin-17 signaling in inflammatory, Kupffer cells, and hepatic stellate cells exacerbates liver fibrosis in mice. Gastroenterology 143: 765-776.e3, 2012.
57. Zhang Y, Huang D, Gao W, Yan J, Zhou W, Hou X, Liu M, Ren C, Wang S and Shen J: Lack of IL-17 signaling decreases liver fibrosis in murine *Schistosomiasis japonica*. Int Immunol 27: 317-325, 2015.
58. Hyun J, Wang S, Kim J, Rao KM, Park SY, Chung I, Ha CS, Kim SW, Yun YH and Jung Y: MicroRNA-378 limits activation of hepatic stellate cells and liver fibrosis by suppressing Gli3 expression. Nat Commun 7: 10993, 2016.
59. Sunaga H, Matsui H, Ueno M, Maeno T, Iso T, Syamsunarno MR, Anjo S, Matsuzaka T, Shimano H, Yokoyama T and Kurabayashi M: Deranged fatty acid composition causes pulmonary fibrosis in Elovl6-deficient mice. Nat Commun 4: 2563, 2013.
60. Shiu TY, Huang SM, Shih YL, Chu HC, Chang WK and Hsieh TY: Correction: Hepatitis C virus core protein down-regulates p21Waf1/Cip1 and inhibits curcumin-induced apoptosis through MicroRNA-345 targeting in human hepatoma cells. PLoS One 12: e0181299, 2017.
61. Shen G, Rong X, Zhao J, Yang X, Li H, Jiang H, Zhou Q, Ji T, Huang S, Zhang J and Jia H: MicroRNA-105 suppresses cell proliferation and inhibits PI3K/AKT signaling in human hepatocellular carcinoma. Carcinogenesis 35: 2748-2755, 2014.
62. An F, Gong B, Wang H, Yu D, Zhao G, Lin L, Tang W, Yu H, Bao S and Xie Q: miR-15b and miR-16 regulate TNF mediated hepatocyte apoptosis via BCL2 in acute liver failure. Apoptosis 17: 702-716, 2012.
63. Koo JH, Lee HJ, Kim W and Kim SG: Endoplasmic reticulum stress in hepatic stellate cells promotes liver fibrosis via PERK-mediated degradation of HNRNPA1 and up-regulation of SMAD2. Gastroenterology 150: 181-193.e8, 2016.
64. Du K, Oh SH, Dutta RK, Sun T, Yang WH, Chi JT and Diehl AM: Inhibiting xCT/SLC7A11 induces ferroptosis of myofibroblastic hepatic stellate cells but exacerbates chronic liver injury. Liver Int 41: 2214-2227, 2021.
65. Zhang L, Huang Y, Ling J, Zhuo W, Yu Z, Luo Y and Zhu Y: Overexpression of SLC7A11: A novel oncogene and an indicator of unfavorable prognosis for liver carcinoma. Future Oncol 14: 927-936, 2018.
66. Lodder J, Denaës T, Chobert MN, Wan J, El-Benna J, Pawlotsky JM, Lotersztajn S and Teixeira-Clerc F: Macrophage autophagy protects against liver fibrosis in mice. Autophagy 11: 1280-1292, 2015.
67. Eferl R, Hasselblatt P, Rath M, Popper H, Zenz R, Komnenovic V, Idarraga MH, Kenner L and Wagner EF: Development of pulmonary fibrosis through a pathway involving the transcription factor Fra-2/AP-1. Proc Natl Acad Sci USA 105: 10525-10530, 2008.
68. Rajalingam K, Schreck R, Rapp UR and Albert S: Ras oncogenes and their downstream targets. Biochim Biophys Acta 1773: 1177-1195, 2007.
69. Llovet JM, Zucman-Rossi J, Pikarsky E, Sangro B, Schwartz M, Sherman M and Gores G: Hepatocellular carcinoma. Nat Rev Dis Primers 2: 16018, 2016.
70. Carlson CM, Frandsen JL, Kirchhof N, McIvor RS and Largaespada DA: Somatic integration of an oncogene-harboring sleeping beauty transposon models liver tumor development in the mouse. Proc Natl Acad Sci USA 102: 17059-17064, 2005.
71. Rudalska R, Dauch D, Longerich T, McJunkin K, Wuestefeld T, Kang TW, Hohmeyer A, Pesic M, Leibold J, von Thun A, *et al*: In vivo RNAi screening identifies a mechanism of sorafenib resistance in liver cancer. Nat Med 20: 1138-1146, 2014.
72. Yue C, Ren Y, Ge H, Liang C, Xu Y, Li G and Wu J: Comprehensive analysis of potential prognostic genes for the construction of a competing endogenous RNA regulatory network in hepatocellular carcinoma. Onco Targets Ther 12: 561-576, 2019.

73. Zhang L, Huang Y, Zhu Y, Yu Z, Shao M and Luo Y: Identification and characterization of cadmium-related genes in liver carcinoma. Biol Trace Elem Res 182: 238-247, 2018.
74. Divella R, Mazzocca A, Gadaleta C, Simone G, Paradiso A, Quaranta M and Daniele A: Influence of plasminogen activator inhibitor-1 (SERPINE1) 4G/5G polymorphism on circulating SERPINE-1 antigen expression in HCC associated with viral infection. Cancer Genomics Proteomics 9: 193-198, 2012.
75. Czekay RP, Aertgeerts K, Curriden SA and Loskutoff DJ: Plasminogen activator inhibitor-1 detaches cells from extracellular matrices by inactivating integrins. J Cell Biol 160: 781-791, 2003.
76. Roca C, Primo L, Valdembri D, Cividalli A, Declerck P, Carmeliet P, Gabriele P and Bussolino F: Hyperthermia inhibits angiogenesis by a plasminogen activator inhibitor 1-dependent mechanism. Cancer Res 63: 1500-1507, 2003.
77. Wu B, Wang Y, Yang XM, Xu BQ, Feng F, Wang B, Liang Q, Li Y, Zhou Y, Jiang JL and Chen ZN: Basigin-mediated redistribution of CD98 promotes cell spreading and tumorigenicity in hepatocellular carcinoma. J Exp Clin Cancer Res 34: 110, 2015.
78. Wang L, Zhang Z, Li M, Wang F, Jia Y, Zhang F, Shao J, Chen A and Zheng S: P53-dependent induction of ferroptosis is required for artemether to alleviate carbon tetrachloride-induced liver fibrosis and hepatic stellate cell activation. IUBMB Life 71: 45-56, 2019.
79. Ghosh AK and Vaughan DE: PAI-1 in tissue fibrosis. J Cell Physiol 227: 493-507, 2012.
80. Ji J, Yu F, Ji Q, Li Z, Wang K, Zhang J, Lu J, Chen L, E Q, Zeng Y and Ji Y: Comparative proteomic analysis of rat hepatic stellate cell activation: A comprehensive view and suppressed immune response. Hepatology 56: 332-349, 2012.
81. Khambu B, Yan S, Huda N, Liu G and Yin XM: Autophagy in non-alcoholic fatty liver disease and alcoholic liver disease. Liver Res 2: 112-119, 2018.
82. Gao M and Liu D: CRISPR/Cas9-based Pten knock-out and sleeping beauty transposon-mediated Nras knock-in induces hepatocellular carcinoma and hepatic lipid accumulation in mice. Cancer Biol Ther 18: 505-512, 2017.
83. Cao W, Li Y, Li M, Zhang X and Liao M: Txn1, Ctsd and Cdk4 are key proteins of combination therapy with taurine, epigallocatechin gallate and genistein against liver fibrosis in rats. Biomed Pharmacother 85: 611-619, 2017.
84. Li R, Wang Y, Song X, Sun W, Zhang J, Liu Y, Li H, Meng C, Zhang J, Zheng Q and Lv C: Potential regulatory role of circular RNA in idiopathic pulmonary fibrosis. Int J Mol Med 42: 3256-3268, 2018.